communications biology

Article

https://doi.org/10.1038/s42003-024-07296-x

Interactions between excitatory neurons and parvalbumin interneurons in V1 underlie neural mechanisms of amblyopia and visual stimulation treatment

Yiru Huang[1,4], Zitian Liu[1,4], Zongyi Zhan[2], Xinyi Zhang[1], Le Gao[1], Mingqin Wang[1], Yixiao Fu[1], Lianyan Huang[3] ✉ & Minbin Yu[1] ✉

As the main cause of visual function deficits in children and adolescents worldwide, amblyopia causes serious impairment of monocular visual acuity and stereopsis. The recovery of visual functions from amblyopia beyond the critical period is slow and incomplete due to the limited plasticity of the mature cortex; notably, visual stimulation training seems to be an effective therapeutic strategy in clinical practice. However, the precise neural basis and cellular mechanisms that underlie amblyopia and visual stimulation treatment remain to be elucidated. Using monocular deprivation in juvenile mice to model amblyopia, we employed two-photon calcium imaging and chemogenetic techniques to investigate the visual responses of individual excitatory neurons and parvalbumin (PV^+) interneurons in the primary visual cortex (V1) of amblyopic mice. We demonstrate that amblyopic mice exhibit an excitation/inhibition (E/I) imbalance. Moreover, visual stimulation decreases the response of PV^+ interneurons, reactivates the ocular dominance plasticity of excitatory neurons, and promotes vision recovery in adult amblyopic mice. Our results reveal a dynamic E/I balance between excitatory neurons and PV^+ interneurons that may underlie the neural mechanisms of amblyopia during cortical development and visual stimulation-mediated functional recovery from adult amblyopia, providing evidence for therapeutic applications that rely on reactivating adult cortical plasticity.

Visual cortex plasticity, the capacity of the visual cortex to undergo experience-dependent changes in synaptic strength and circuit connectivity during postnatal development, is dynamically regulated, with plasticity peaking during the critical period and then decreasing with maturation[1–3]. Abnormal visual experiences in early life, such as strabismus, anisometropia, high refractive error, and congenital cataract, may cause amblyopia—a loss of visual acuity and binocular vision functions affecting 1–3% of the population[4,5]. As the main cause of visual function deficits in children and adolescents worldwide, amblyopia leads to lifelong deficiencies in visual acuity and stereopsis without timely and appropriate treatment, seriously affecting patients' psychosocial health and quality of life[6–8]. Since the 1700s, the clinical treatment for amblyopia has consisted of patching or penalizing the strong eye to force the "lazy" amblyopic eye to work. This treatment has generally been restricted to infants and young children during the critical period but seems to be useless for older children and adult patients due to the limited plasticity of the mature cortex[9]. Recent research[10,11] and our previous studies[12–14] have suggested that intensive visual stimulation training, i.e., perceptual learning, aimed at reducing the inhibition of the amblyopic eye by the strong fellow eye and enhancing binocular fusion, is a therapeutic strategy for recovery in older children and adults with amblyopia. However, the results from several randomized clinical trials on the effects of perceptual learning or video game play are contradictory[15–17]. To better understand the reasons for these mixed results, improve clinical treatment strategies for amblyopia, and enhance the effects of visual stimulation training, we focus our research on the nature and neural mechanisms underlying amblyopia and visual training treatment, which remain largely unknown.

[1]State Key Laboratory of Ophthalmology, Zhongshan Ophthalmic Center, Sun Yat-sen University, Guangdong Provincial Key Laboratory of Ophthalmology and Visual Science, Guangzhou, Guangdong, China. [2]Shenzhen Eye Hospital, Shenzhen Eye Institute, Shenzhen Eye Hospital affiliated to Jinan University, Shenzhen, Guangdong, China. [3]Department of Pathophysiology, Zhongshan School of Medicine, Sun Yat-sen University, Guangzhou, Guangdong, China. [4]These authors contributed equally: Yiru Huang, Zitian Liu. ✉e-mail: huangly55@mail.sysu.edu.cn; yuminbin@mail.sysu.edu.cn

Monocular deprivation (MD) during early life causes a progressive loss of neuronal responsiveness in the primary visual cortex (V1) through the deprived eye (e.g., ocular dominance plasticity and orientation selectivity) and has been used in animal models of amblyopia to explore the experience-dependent plasticity[18,19]. Experiments in amblyopic animals have shown that under certain conditions (e.g., with identical contrast, spatial frequency, and temporal features), binocular visual experience can promote ocular dominance plasticity and restore visual functions[20–22]. Although the neural mechanisms underlying visual stimulation treatment for amblyopia remain unclear, neural circuit plasticity regulated by the balance of excitation and inhibition (E/I) is a potential explanation. The E/I balance is believed to be a major mechanism by which cortical networks adapt to sensory input[23–27]. Increased inhibition exerted by the maturation of parvalbumin-expressing basket interneurons (PV^+ interneurons) has been demonstrated to trigger critical-period plasticity in the visual cortex[28–30]. Brief MD during the critical period evokes a rapid loss of excitatory synaptic inputs to PV^+ interneurons, thus reducing the inhibition to excitatory glutamatergic neurons, and causing cortical disinhibition and juvenile visual cortical plasticity via the downregulation of neuregulin-1(NRG1)/ErbB4 signaling in PV^+ interneurons[31,32]. In addition, perineuronal nets (PNNs) are specialized extracellular matrix structures that predominantly surround and stabilize PV^+ interneurons[33,34]. PNNs progressively aggregate during postnatal development as structural obstacles to ocular dominance plasticity, in parallel with the closure of the critical period[35–37]. Moreover, Shmal et al. found that knockdown of the transcriptional repressor REST restores V1 plasticity and rescues vision in adult amblyopic mice, outcomes that are associated with a reduction in PNNs around PV^+ interneurons[38]. However, what changes occur in the V1 network (e.g., visual responses of individual excitatory or inhibitory neurons) in amblyopia induced by early-onset, long-term MD and how visual stimulation treatment can restore vision from amblyopia based on limited plasticity beyond the cortical period remain unclear.

To address these questions, we employed two-photon calcium imaging and chemogenetic techniques in an amblyopic mouse model to investigate the visual responses of individual excitatory neurons and PV^+ interneurons in V1. We observed an excitation/inhibition (E/I) imbalance in V1 of amblyopic mice, which specifically manifested as an obvious ocular dominance shift, decreased orientation selectivity of excitatory neurons, an enhanced response of PV^+ interneurons and increased density of PNNs surrounding PV^+ interneurons after 30 days of MD starting from the critical period. Furthermore, we investigated the beneficial effects of visual stimulation on vision recovery and found that visual stimulation training reactivated ocular dominance plasticity and increased visual acuity in adult amblyopic mice by reducing the PV^+ interneuron response. Together, our findings indicate a dynamic E/I balance between excitatory neurons and PV^+ interneurons that underlies the neural mechanisms of amblyopia and visual stimulation-mediated functional recovery from adult amblyopia, suggesting potential alternative strategies for the treatment of amblyopia in clinical practice.

Results

Amblyopic mice show an ocular dominance shift and reduced orientation selectivity of V1 excitatory neurons

Using long-term MD in juvenile mice to model amblyopia, we first measured the change in visual acuity thresholds induced by 30 days of MD (from P28 to P58[39]). The visual acuity threshold, which approximates the maximum spatial frequency of the grating visual stimuli sufficient to elicit an optomotor response (OMR), was obtained from mice in the MD group and an age-matched normal control (NC) group. The plasticity of the OMR was previously believed to be based mainly on subcortical circuitry[40,41]. However, new research on cortical lesions suggests that the visual cortex may also be involved[42–44]. To measure OMRs, the head movements of the unrestrained tested animal were video-recorded by a camera placed above the animal and analyzed by an algorithm that tracks the position of the mouse's head. According to the analysis modified from a previously published version[45], we found that the visual acuity thresholds of the left (MD) eyes of MD-treated mice were significantly lower than those of NC mice (Fig. 1b), and the mean visual acuity thresholds were 0.241 ± 0.046 cyc/° and 0.349 ± 0.050 cyc/°, respectively. For the right eye, no significant difference was observed between the NC and MD groups (Fig. 1b). These results suggest that long-term MD can impair visual acuity, effectively simulating the visual impairment caused by amblyopia to a certain extent.

Then, we carried out in vivo two-photon calcium imaging (2-P imaging) in Thy1-GCaMP6s transgenic mice that expressed the green fluorescent calcium indicator GCaMP6s in excitatory neurons. Calcium imaging was performed in layer L2/3 of the V1 binocular zone (V1b) of awake mice viewing drifting gratings of various orientations. Stimuli were presented to either the right or left eye, for the hemisphere contralateral (i.e., right side) to the original deprived eye (Fig. 1c). Amblyopic mice in the MD group and littermate NCs were used to assess the visual responses of individual excitatory neurons in V1b. Compared with NC mice, amblyopic mice manifested a large shift in the ocular dominance index (ODI) in favor of the ipsilateral eye, from 0.122 ± 0.292 in the NC group to −0.047 ± 0.336 in the MD group (Fig. 1e, f), which is consistent with earlier studies reporting that the ODI of excitatory neurons shifted from 0.185 ± 0.017 in normally reared control mice to −0.033 ± 0.015 in experimental mice at the end of 30 days of MD[39]. The ODI shift was achieved mainly by a change in the nondeprived-eye input, with the response ($\Delta F/F_0$) to stimulation of the ipsilateral eye increasing after 30 days of MD compared with that observed in NC mice. A corresponding decrease in the response to stimulation of the contralateral eye was observed after 30 days of MD, but the difference did not reach significance (Fig. 1g). In addition, the orientation selectivity index (OSI) to the contralateral eye decreased significantly, from 0.283 ± 0.177 for the NC group to 0.208 ± 0.158 for the MD group, as did the OSI to the ipsilateral eye, which decreased from 0.212 ± 0.156 to 0.171 ± 0.116 (Fig. 1J). These findings are partially consistent with the conclusion reported by Craddock et al.[46], showing that the OSI for the contralateral eye in the V1b of young adult mice (2–3 months) decreases, whereas the OSI for the ipsilateral eye increases (although it fails to reach significance) after 2 weeks of MD, which we speculate may be due to the differences in age groups and durations of MD in mice. In general, we found that relative to the excitatory neurons recorded from NC mice, amblyopic mice induced by long-term MD displayed an obvious ocular dominance shift toward the ipsilateral eye and reduced orientation selectivity of the excitatory neurons in V1.

Amblyopic mice exhibit an enhanced response of PV^+ interneurons and an increased density of PNNs surrounding PV^+ interneurons

We further investigated the changes in a major type of GABAergic interneurons, PV^+ inhibitory neurons, in amblyopic mice. To identify the PV^+ interneurons in V1b, Cre-dependent rAAV-Ef1α-DIO-GCaMP6f was used to drive green fluorescence expression in PV^+ interneurons of PV^{Cre} mice and observed by in vivo two-photon calcium imaging (Fig. 2a). The results showed that PV^+ interneurons exhibited a mild contralateral ODI bias in the NC group (0.101 ± 0.510) and a weaker OD shift toward the ipsilateral eye than excitatory neurons did after 30 days of MD (0.081 ± 0.372; Fig. 2b, c). In addition, the OSIs of PV^+ interneurons were low in the NC mice (Contra: 0.173 ± 0.148; Ipsi: 0.193 ± 0.145) and did not change significantly in the MD-treated mice (Contra: 0.151 ± 0.102; Ipsi: 0.173 ± 0.112; Fig. 2e, f). Interestingly, the responses of PV^+ interneurons to stimulation of both the contralateral and ipsilateral eyes of amblyopic mice in the MD group were greater than those in the NC group (Fig. 2d), indicating that long-term MD enhances the response of PV^+ interneurons in amblyopic mice.

We also estimated the density of PV^+ interneurons and the related PNNs in brain sections from amblyopic and NC mice (5 mice per group). Figure 2g shows representative examples of results obtained from one animal in the NC or MD group. The densities of PV^+ interneurons and PNNs in the contralateral (right side) V1 region were observed and compared. No significant difference in the absolute number of PV^+ interneurons was observed between the NC and MD groups (Fig. 2h); however, the number of PV^+ interneurons surrounded by PNNs increased in amblyopic

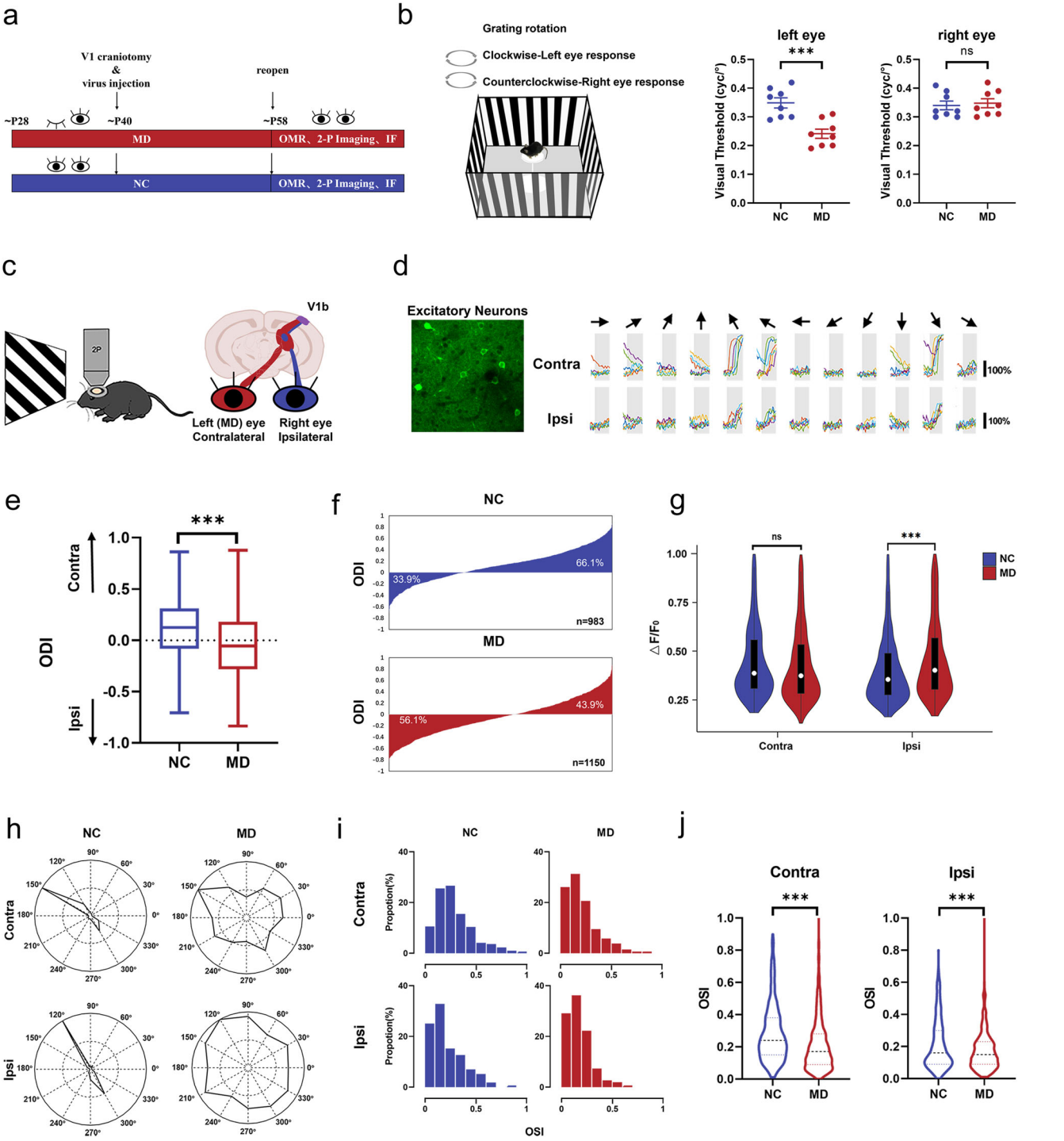

mice (Fig. 2i). Specifically, the percentage of PV$^+$ interneurons surrounded by PNNs was 42.82 ± 3.02% (mean ± SEM) in the NC group but increased to 58.92 ± 2.51% in the MD group (Fig. 2j). The percentage of area covered by PNNs in V1 and the mean intensity of the fluorescence of WFA staining for PNNs also showed similar increases in amblyopic mice (Fig. 2k, l).

Previous studies have reported a reduction in the PV$^+$ interneuron response after brief MD during the critical period[28,47] and a significant decrease in the expression of PNNs surrounding PV$^+$ interneurons after visual deprivation caused by dark exposure[48,49]. However, we found that long-term MD-induced amblyopic mice exhibit an enhanced response in PV$^+$ interneurons and an increased density of PNNs surrounding PV$^+$ interneurons. Considering the important regulatory role of PV$^+$ interneurons in the activity of excitatory neurons and cortical inhibition[24,31], and the association of PNNs with neural stability and plasticity inhibition[33,50], our results imply that the increased response of PV$^+$ interneurons and enhanced inhibition to excitatory neurons may disrupt the balance of excitation and inhibition in V1 and thus underlie the neural mechanism of amblyopia.

Inhibition of PV$^+$ interneurons reverses the MD-induced ocular dominance shift and promotes vision recovery in amblyopic mice

To further verify the imbalance of excitation and inhibition in amblyopic mice, we tested whether the inhibition of PV$^+$ interneurons could promote synaptic plasticity and vision recovery in an MD-induced amblyopia-like

Fig. 1 | Amblyopic mice show an ocular dominance shift and reduced orientation selectivity of V1 excitatory neurons. a Experimental timeline. Mice underwent 30 days of MD via lid suturing of the left eye from P28 to P58. Cranial window surgery and/or virus injection surgery were performed two to three weeks before reopening the deprived eye. Both MD mice and age-matched NC mice without prior manipulation of vision were recorded at P58. Visual acuity thresholds were assessed by measuring the optomotor response (OMR), and visual cortical responses were recorded by in vivo two-photon (2-P) calcium imaging. Tissue sections of the visual cortex were prepared for immunofluorescence (IF) staining. **b** Schematic of the OMR arena used for the visual acuity measurement, and the visual acuity thresholds of the left ($t = 4.471$, $p < 0.001$) or right ($t = 0.343$, $p = 0.737$) eyes of the mice in the NC and MD groups ($n = 8$ mice/group). **c** Illustration of in vivo two-photon calcium imaging performed in the right V1b of awake, head-fixed mice. The stimuli were presented to either the left (contralateral) or right (ipsilateral) eyes. **d** A maximum-intensity image of V1 excitatory neurons expressing GCaMP6s and visual responses of individual neurons to stimulation of the contralateral or ipsilateral eye when drifting gratings of various orientations were presented. **e** Comparisons of the ODIs of V1 excitatory neurons. The solid line within each box represents the median. The box represents the interquartile range (IQR) of the data (25th percentile to 75th percentile). NC: $n = 983$ neurons; MD: $n = 1150$ neurons. $t = 12.30$, $p < 0.001$. **f** Distributions of the ODI and the percentage of excitatory neurons whose ODI is above (contralateral bias) or below (ipsilateral bias) zero. **g** Violin plots and overlaid box plots of the response amplitude ($\Delta F/F_0$) of V1 excitatory neurons. Contra: $t = 1.895$, $p = 0.058$; Ipsi: $t = 6.071$, $p < 0.001$. **h** Representative polar plots of the responses to drifting gratings of the contralateral or ipsilateral eye from an excitatory neuron of each group. **i** Population distributions of the OSI of V1 excitatory neurons. **j** Comparisons of the OSI of V1 excitatory neurons. The dashed lines in the violin plots represent the 25% quartiles, median, and 75% quartile. Contra: $t = 7.437$, $p < 0.001$; Ipsi: $t = 5.270$, $p < 0.001$. For all figures: two-tailed independent samples t-tests were used to compare the NC and MD groups; $^{**}p < 0.01$; $^{***}p < 0.001$; ns no significant difference. The error bars indicate the SEMs. Contra contralateral, Ipsi ipsilateral.

model. We selectively manipulated the activity of PV^+ interneurons using a chemogenetic technique, designer receptors exclusively activated by designer drugs (DREADDs)[31]. Offspring of Thy1-GCaMP6s transgenic mice crossed with PV^{Cre} mice (Thy1-GCaMP6s; PV^{Cre} mice) were monocularly deprived from P28 to P58 and were microinjected with an adeno-associated virus (AAV) expressing Cre-dependent hM4Di receptor (hM4Di group) in the right V1 two to three weeks before reopening the left eye. AAV-hSyn-DIO-mCherry was also injected as the control vector (mCherry group). The activity of V1 PV^+ interneurons was selectively inhibited daily via i.p. injection of clozapine N-oxide (CNO, 0.3 mg/kg) for seven days after reopening the left eye in both the hM4Di group and the mCherry group (Fig. 3a, b). The measurements (OMR and 2-P imaging) were conducted on the second day after the end of the injection to ensure that CNO was completely washed out.

We found that chemogenetic inhibition of PV^+ interneurons significantly promoted vision recovery from amblyopia with a higher visual acuity threshold (0.309 ± 0.024 cyc/°) than that in the mCherry group (0.263 ± 0.030 cyc/°; Fig. 3c, Supplementary Fig. 1) after 7 days of CNO injection, although it did not return to the level of normal mice (approximately 50% recovery). In addition, V1b ocular dominance returned to a distribution of contralateral bias, similar to that of NC mice, after 7 days of PV^+ interneuron inhibition. In the hM4Di group, the ODI was significantly greater (0.093 ± 0.323) than that in the mCherry group (0.001 ± 0.232; Fig. 3d, e), with a significantly increased contralateral eye response and a decreased ipsilateral eye response of V1 excitatory neurons compared with those in the mCherry group (Fig. 3f), indicating a preference for the contralateral eye. The OSI of V1 excitatory neurons was also greater in the hM4Di group (Fig. 3h, i). In terms of the densities of PV^+ interneurons and PNNs in the contralateral V1 region, no significant difference in the absolute number of PV^+ interneurons or the number of PV^+ interneurons surrounded by PNNs was observed between the hM4Di and mCherry groups (Fig. 3k–m). However, the percentage of area covered by PNNs and the mean intensity of the fluorescence of WFA staining for PNNs in the V1 region were lower in the hM4Di group than those in the mCherry group (Fig. 3n, o). These results confirmed the imbalance of excitation and inhibition in amblyopic mice. Moreover, our findings suggested that the inhibition of PV^+ interneurons could reverse the effects of long-term MD and reactivate ocular dominance plasticity in amblyopic mice so that they could achieve better vision recovery, consistent with previous reports by Kuhlman et al.[28] that the pharmacogenetic reduction in PV^+ interneuron firing rates can extend the critical period for ocular dominance plasticity.

Visual stimulation training reactivates ocular dominance plasticity and promotes vision recovery in adult amblyopic mice

Based on the changes in excitation/inhibition imbalance in amblyopia that we mentioned above, we further explored whether visual stimulation could improve vision functions by restoring the E/I balance. We randomly assigned amblyopic mice after long-term MD into two groups: one group received grating visual stimulation for seven days (VS+ group), and the other group did not (VS− group). Visual stimulation training was also carried out in the OMR arena with binocular presentation. To optimize the potential for recovery of binocular responses, from P58 to P65, the mice in the VS+ group were placed in the chamber surrounded by four LED monitors presenting high-contrast, phase-reversing gratings matched to the spatiotemporal frequency response of the mouse (12 orientations, 0.05 cycles/degree, reversing at 1 Hz, Fig. 4a) in an interleaved manner for 1 h/day during daylight for seven consecutive days. This type of visual stimulus was selected to mimic visual stimuli used experimentally to promote optimal recovery from MD in adult mice[51,52] and amblyopia patients[11,15,53].

We found that the mean visual acuity threshold of the left (MD) eye in the VS+ group (0.289 ± 0.023 cyc/°) was significantly greater than that in the VS− group (0.246 ± 0.029 cyc/°), but no significant difference in the visual acuity threshold of the right eye was found between the VS+ and VS− groups (Fig. 4b). In addition, the vision-promoting effects of visual stimulation training (1 hour/day, 7 days) lasted for at least 2 weeks after training was terminated (Supplementary Fig. 2A). To further determine whether multiple days of visual stimulation are required to promote vision recovery, we compared the effects of 1 day, 3 days, 1 week, and 2 weeks of visual stimulation training (1 h/day) on the visual acuity threshold and found that the vision-promoting effects of visual stimulation training appeared to be dose-dependent; at least 1 week of visual stimulation training was needed to significantly promote vision recovery (Supplementary Fig. 2B). These results confirmed that long-term exposure to grating visual stimulation promotes vision recovery in adult amblyopic mice.

To further explore the neural mechanisms underlying the ability of visual stimulation to restore vision from amblyopia based on limited plasticity beyond the cortical period, we carried out in vivo two-photon calcium imaging to observe the visual responses of individual excitatory neurons and PV^+ interneurons in V1 of mice in the VS+ and VS− groups. We found that seven days of visual stimulation training increased the ODI of V1 excitatory neurons to 0.051 ± 0.287 and returned V1 ocular dominance to a contralateral eye preference. In contrast, the ocular dominance distributions of mice without grating visual stimulation still showed an ipsilateral eye bias, and the ODI was maintained at -0.030 ± 0.317, suggesting poor recovery from long-term MD compared with that in the VS+ group (Fig. 4c, d). Compared with that in the VS− group, the response of excitatory neurons to stimulation of the ipsilateral eye was significantly decreased after 7 days of visual stimulation training, whereas the response to the contralateral eye was not significantly different between the VS+ and VS− groups (Fig. 4e). In addition, compared with those in the VS− group, the OSIs of both the contralateral and ipsilateral eyes were significantly greater in the VS+ group, with values of 0.243 ± 0.166 and 0.275 ± 0.152 to the contralateral eye and 0.168 ± 0.132 and 0.190 ± 0.119 to the ipsilateral eye, respectively (Fig. 4g, h). Taken together, these results indicate that visual stimulation training reactivates ocular dominance plasticity and promotes vision recovery in adult amblyopic mice.

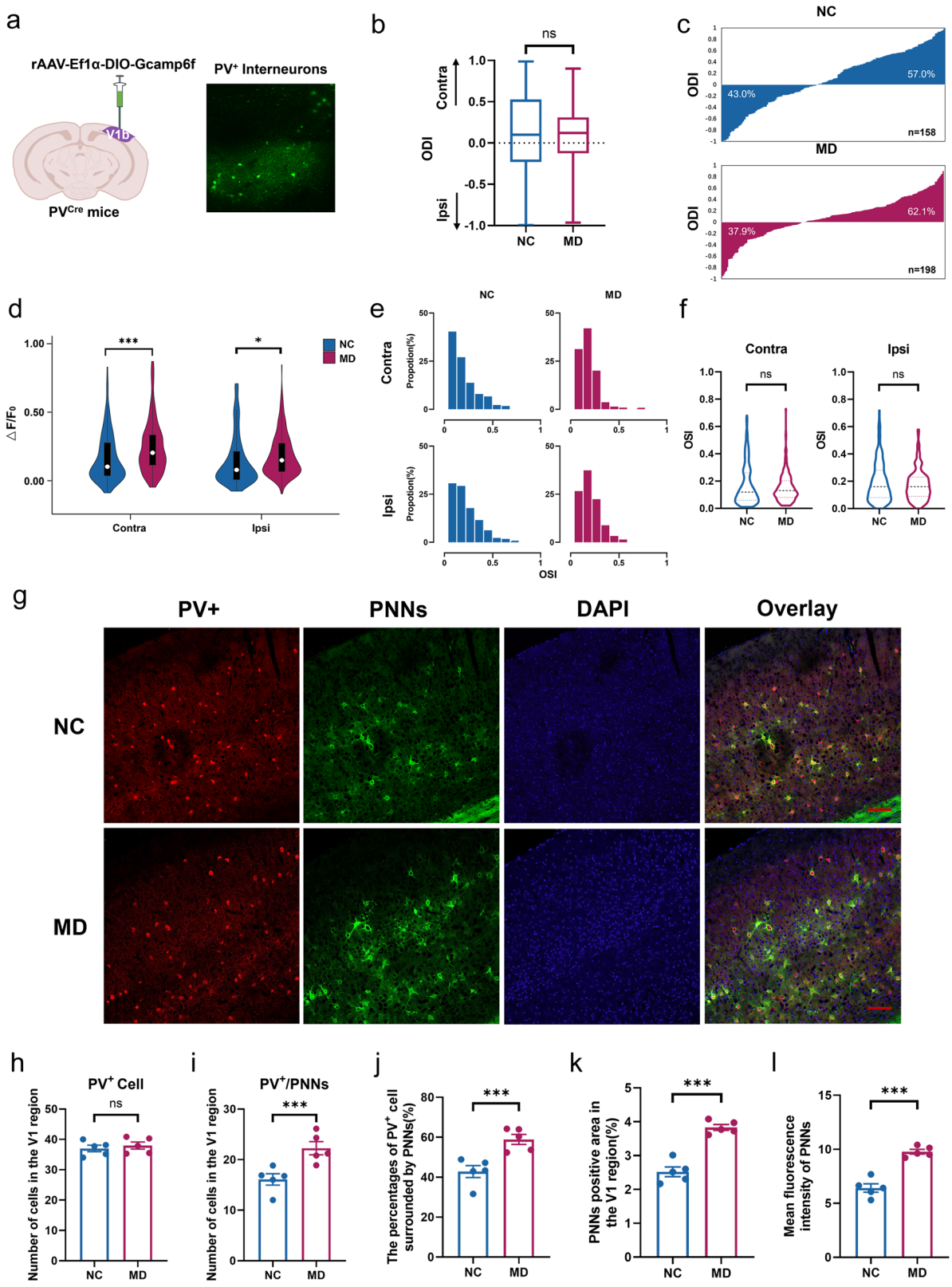

Visual stimulation training decreases the response of PV$^+$ interneurons and the density of PNNs surrounding PV$^+$ interneurons in adult amblyopic mice

We also observed the visual response of V1 PV$^+$ interneurons in adult amblyopic mice after 7 days of visual stimulation training and found that the ODI of PV$^+$ interneurons in the VS+ group (0.096 ± 0.500) was not significantly different from that in the VS− group (0.062 ± 0.451; Fig. 5a, b). The OSIs of both contralateral and ipsilateral eyes in the two groups were not different (Fig. 5d, e). However, the responses of PV$^+$ interneurons to stimulation of the contralateral and ipsilateral eyes decreased after 7 days of visual stimulation training in the VS+ group compared with those in the VS− group (Fig. 5c), suggesting that visual

Fig. 2 | Amblyopic mice show an enhanced response of PV$^+$ interneurons and an increased density of PNNs surrounding PV$^+$ interneurons. **a** Illustration of the specific infection of V1 PV$^+$ interneurons with GCaMP6f and an in vivo two-photon calcium image of V1 PV$^+$ interneurons expressing GCaMP6f. **b** Comparisons of the ODI of V1 PV$^+$ interneurons. NC: $n = 158$ neurons; MD: $n = 198$ neurons. $t = 0.417$, $p = 0.677$. **c** Distributions of the ODI and the percentage of PV$^+$ interneurons whose ODI is above (contralateral bias) or below (ipsilateral bias) zero. **d** Violin plots and overlaid box plots of the response amplitude of V1 PV$^+$ interneurons. Contra: $t = 4.043$, $p < 0.001$; Ipsi: $t = 2.079$, $p = 0.038$. **e** Population distributions of the OSI of V1 PV$^+$ interneurons. **f** Comparisons of the OSI of V1 PV$^+$ interneurons. Contra: $t = 1.827$, $p = 0.068$; Ipsi: $t = 1.611$, $p = 0.108$. **g** Representative fluorescence photomicrographs of coronal V1 sections from one animal in each group ($n = 5$ mice/group). Scale bar, 50 μm. **h** Density of PV$^+$ interneurons. $t = 0.607$, $p = 0.561$. **i** Density of PV$^+$ interneurons surrounded by PNNs. $t = 5.226$, $p < 0.001$. **j** Percentages of PV$^+$ interneurons surrounded by PNNs. $t = 4.630$, $p < 0.001$. **k** PNNs-stained area. $t = 7.831$, $p < 0.001$. **l** The mean intensity of PNNs fluorescence. $t = 7.553$, $p < 0.001$. For all figures: two-tailed independent samples t-tests were used to compare the NC and MD groups; $^*p < 0.05$; $^{***}p < 0.001$; ns no significant difference. The error bars indicate the SEMs.

stimulation training decreased the response of PV$^+$ interneurons in adult amblyopic mice.

The results from immunofluorescence staining of V1 sections revealed no significant change in the absolute number of PV$^+$ interneurons (Fig. 5g). However, the number of PV$^+$ interneurons surrounded by PNNs decreased after 7 days of visual stimulation training (Fig. 5h). In the VS+ group, the percentage of PV$^+$ interneurons surrounded by PNNs was 41.99 ± 2.13%, which was significantly lower than that in the VS− group (58.46 ± 2.16%; Fig. 5i). The percentage of area covered by PNNs in the V1 region and the mean intensity of the fluorescence of WFA staining for PNNs also showed similar decreases after visual stimulation training (Fig. 5j, k). Therefore, we speculate that visual stimulation training induces a significant reduction in the densities of PNNs and PV$^+$ interneurons surrounded by PNNs but not in the absolute number of PV$^+$ interneurons.

Activation of PV$^+$ interneurons offsets the vision-promoting effects of visual stimulation training in adult amblyopic mice

Considering that visual stimulation training decreased the response of PV$^+$ interneurons in adult amblyopic mice, we tested whether long-term activation of PV$^+$ interneurons could interfere with the beneficial effects of visual stimulation training on synaptic plasticity and vision recovery. We selectively activated PV$^+$ interneurons in Thy1-GCaMP6s; PV^{Cre} mice by microinjecting AAV expressing Cre-dependent hM3D(Gq) in the right V1. AAV-hSyn-DIO-mCherry was injected as the control vector. Seven days of visual stimulation training were conducted after the eyes were reopened. The activity of V1 PV$^+$ interneurons was selectively activated daily via i.p. injections of clozapine N-oxide (CNO, 0.3 mg/kg) 30 minutes before daily visual stimulation training in both the hM3Dq- and mCherry- injected groups (Fig. 6a, b). The measurements (OMR and 2-P imaging) were conducted on the second day after the end of visual stimulation training to ensure that CNO was completely washed out.

We found that chemogenetic activation of PV$^+$ interneurons accompanied by visual stimulation training (hM3Dq-VS group) significantly impaired the vision-promoting effects of visual stimulation training, with a lower visual acuity threshold (0.272 ± 0.031 cyc/°) than that of the training group injected with the mCherry virus (mCherry-VS group, 0.305 ± 0.026 cyc/°; Fig. 6c, Supplementary Fig. 3) after 7 days of visual stimulation training. Compared with the mCherry-VS group, the activation of PV$^+$ interneurons in the hM3Dq-VS group prevented the reversal of the ocular dominance shift and caused a sustained ipsilateral bias in the ODI of V1b excitatory neurons (0.055 ± 0.312 and −0.013 ± 0.296, respectively; Fig. 6d, e), with significantly decreased contralateral eye responses and increased ipsilateral eye responses (Fig. 6f) of the excitatory neurons in the hM3Dq-VS group. In addition, the hM3Dq-VS group presented significantly lower OSIs to both the contralateral and ipsilateral eyes of V1b excitatory neurons than those of the mCherry-VS group (Fig. 6h, i).

In terms of the densities of PV$^+$ interneurons and PNNs in the contralateral V1 region, no significant difference in the absolute number of PV$^+$ interneurons or the number of PV$^+$ interneurons surrounded by PNNs was observed between the mCherry-VS and hM3Dq-VS groups (Fig. 6k–m). However, the percentage of area covered by PNNs and the mean intensity of the fluorescence of WFA staining for PNNs were greater in the hM3Dq-VS groups than in the mCherry-VS groups (Fig. 6n, o).

Overall, we propose that visual stimulation treatment decreases the response of PV$^+$ interneurons, which may result in an attenuation of inhibition onto excitatory neurons and restore the E/I balance to enhance cortical plasticity in the primary visual cortex, ultimately promoting vision recovery in adult amblyopic mice.

Discussion

There were two major findings from this study. First, using long-term monocular visual deprivation in juvenile mice to model amblyopia, we find that amblyopic mice exhibit a significant E/I imbalance with an obvious ocular dominance shift, decreased orientation selectivity of excitatory neurons, an enhanced response of PV$^+$ interneurons and increased density of PNNs surrounding PV$^+$ interneurons. The inhibition of PV$^+$ interneurons reverses the effects of long-term MD and reactivates the ocular dominance plasticity in amblyopic mice to achieve better vision recovery. Given that amblyopia is the result of functional maldevelopment of the visual cortex, it is important to understand the neuronal basis and cellular mechanisms of amblyopia to make progress in its treatment[54,55]. Second, based on the above findings, we further investigated the beneficial effects of visual stimulation on vision recovery from amblyopia and found that visual stimulation training reactivates visual cortical plasticity and promotes functional recovery in adult amblyopic mice. Reopening visual cortical plasticity after the critical period depends on a reduction in the PV$^+$ interneuron response, which may result in attenuated inhibition to excitatory neurons and sustained cortical disinhibition to enhance cortical plasticity. Together, our findings reveal a dynamic E/I balance between excitatory neurons and PV$^+$ interneurons during the occurrence and recovery of amblyopia, providing theoretical support and an objective basis for clinical visual training treatment of amblyopia even after the critical period and adding new insights into the effect of visual experience on sensory plasticity.

The neural basis of amblyopia is complex and has been a matter of interest and speculation for years. Although its exact cause is unclear, researchers have attributed amblyopia to enhanced interocular suppression[56,57], increased neural noise[58,59], abnormal topographic representation of receptive fields and undersampling of visual space[60–63], and poor synchronization of neuronal responses and disorganization of neural connections[64–68]. In this study, we focused on neuronal responses and explored the interaction between excitatory neurons and PV$^+$ interneurons in V1 of amblyopic mice using two-photon calcium imaging and chemogenetic techniques. Our results show that the balance of excitation and inhibition regulated by the interaction of excitatory neurons and PV$^+$ interneurons in V1 underlies the neural deficits of amblyopia, which is consistent with previous literature suggesting that the excitation/inhibition balance plays an important regulatory role in the beginning and end of the critical period of visual development[24,28]. We speculate that these neuronal deficits are probably the initial manifestation of visual loss and are subsequently involved in the onset and development of amblyopia.

For primates, functional recovery from amblyopia induced by visual deprivation early in life seems slow and far from complete in adulthood due to the limited plasticity of the mature cortex[19,22]. Previous studies have proposed environmental enrichment (EE) as a highly effective strategy for restoring plasticity in adult animals, eliciting visual acuity and ocular

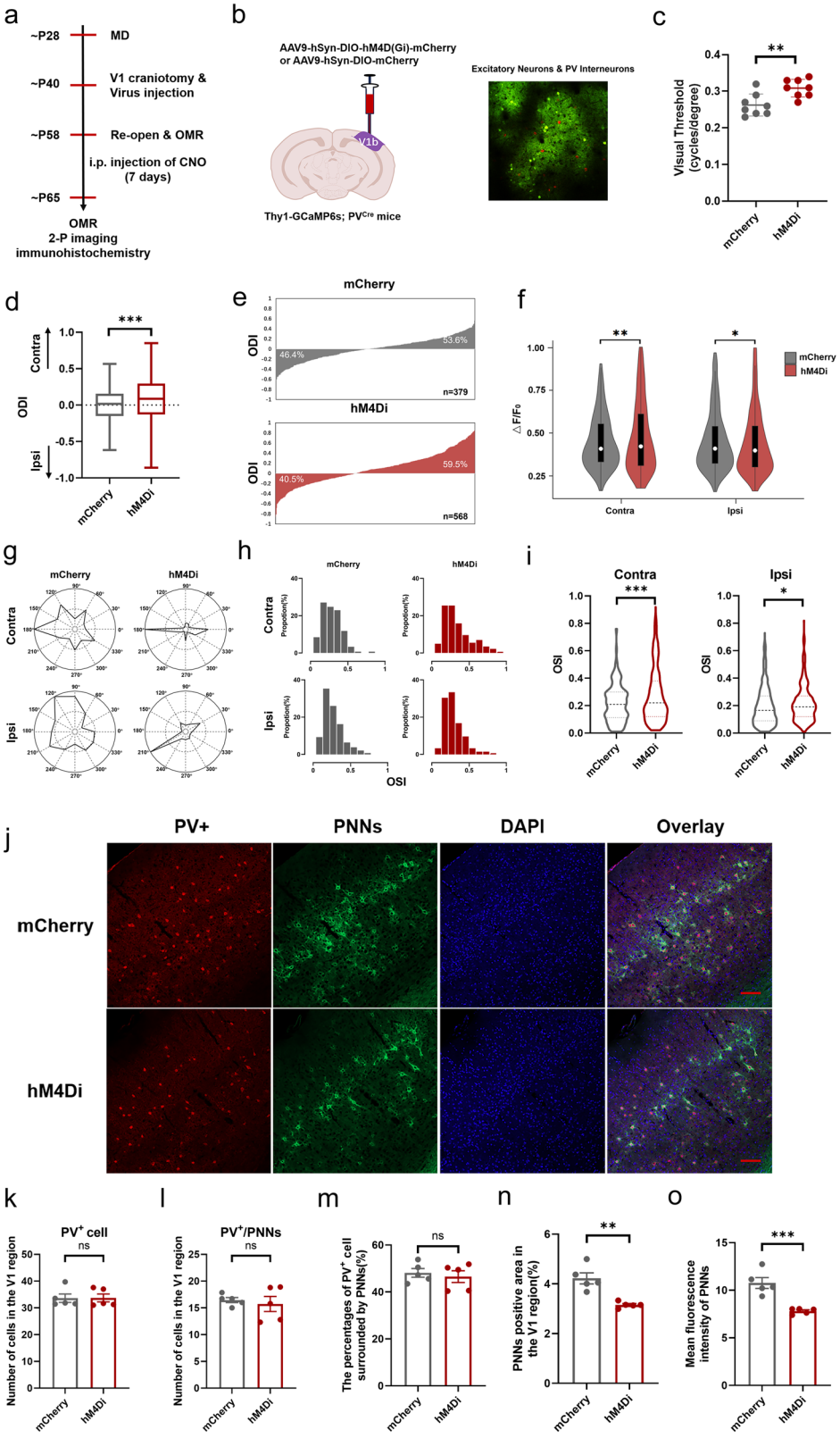

Fig. 3 | Inhibition of PV$^+$ interneurons reverses the MD-induced ocular dominance shift and promotes vision recovery in amblyopic mice. **a** Schematic of the experimental design. **b** Illustration of the specific infection of V1 PV$^+$ interneurons with hM4Di-mCherry or mCherry and an in vivo two-photon calcium image of V1 from a Thy1-GCaMP6s; PV^{Cre} mouse expressing GCaMP6s in excitatory neurons (green) and expressing mCherry in PV$^+$ interneurons (red). **c** Comparisons of the visual acuity thresholds after 7 days of CNO injection ($n = 8$ mice/group) $t = 3.388$, $p = 0.004$. **d** Comparisons of the ODI of V1 excitatory neurons after 7 days of CNO injection. mCherry: $n = 379$ neurons; hM4Di: $n = 568$ neurons. $t = 4.786$, $p < 0.001$. **e** Distribution of the ODI of V1 excitatory neurons and the percentage of excitatory neurons whose ODI is above (contralateral bias) or below (ipsilateral bias) zero. **f** Violin plots and overlaid box plots of the responses of V1 excitatory neurons. Contra: $t = 3.185$, $p = 0.002$; I*p*si: $t = 2.199$, $p = 0.028$. **g** Representative polar plots of responses to drifting gratings of the contralateral or ipsilateral eye from an excitatory neuron of each group. **h** Population distributions of the OSIs of V1 excitatory neurons. **i** Comparisons of the OSI of V1 excitatory neurons. Contra: $t = 4.758$, $p < 0.001$; I*p*si: $t = 2.291$, $p = 0.022$. **j** Representative fluorescence photomicrographs of coronal V1 sections from one animal in each group ($n = 5$ mice/group). Scale bar, 50 μm. **k** Density of PV$^+$ interneurons. $t = 0.038$, $p = 0.971$. **l** Density of PV$^+$ interneurons surrounded by PNNs. $t = 0.492$, $p = 0.636$. **m** Percentages of PV$^+$ interneurons surrounded by PNNs. $t = 0.515$, $p = 0.621$. **n** PNNs-stained area. $t = 4.648$, $p = 0.002$. **o** The mean intensity of PNNs fluorescence. $t = 5.041$, $p < 0.001$. For all figures: two-tailed independent samples t-tests were used to compare the mCherry and hM4Di groups; $^*p < 0.05$; $^{**}p < 0.01$; $^{***}p < 0.001$; ns no significant difference. The error bars indicate the SEMs.

dominance recovery from amblyopia through a reduction in intracortical inhibition[51,69,70]. In this study, using optomotor responses to assess functional changes and in vivo two-photon calcium imaging to record the visual response of individual excitatory neurons in V1 after early-onset, long-term MD, we found that visual stimulation training also dramatically boosts ocular dominance plasticity and increases the visual acuity of adult amblyopic mice. We believe that visual stimulation, a component of environmental enrichment, has similar effects on enhancing ocular dominance plasticity and promoting recovery of vision function as environmental enrichment, both of which are due to reduced GABAergic inhibition in the visual cortex. Matthies et al.[21] reported that 2 days of temporally coherent visual stimuli are sufficient to induce a saturated shift in ocular

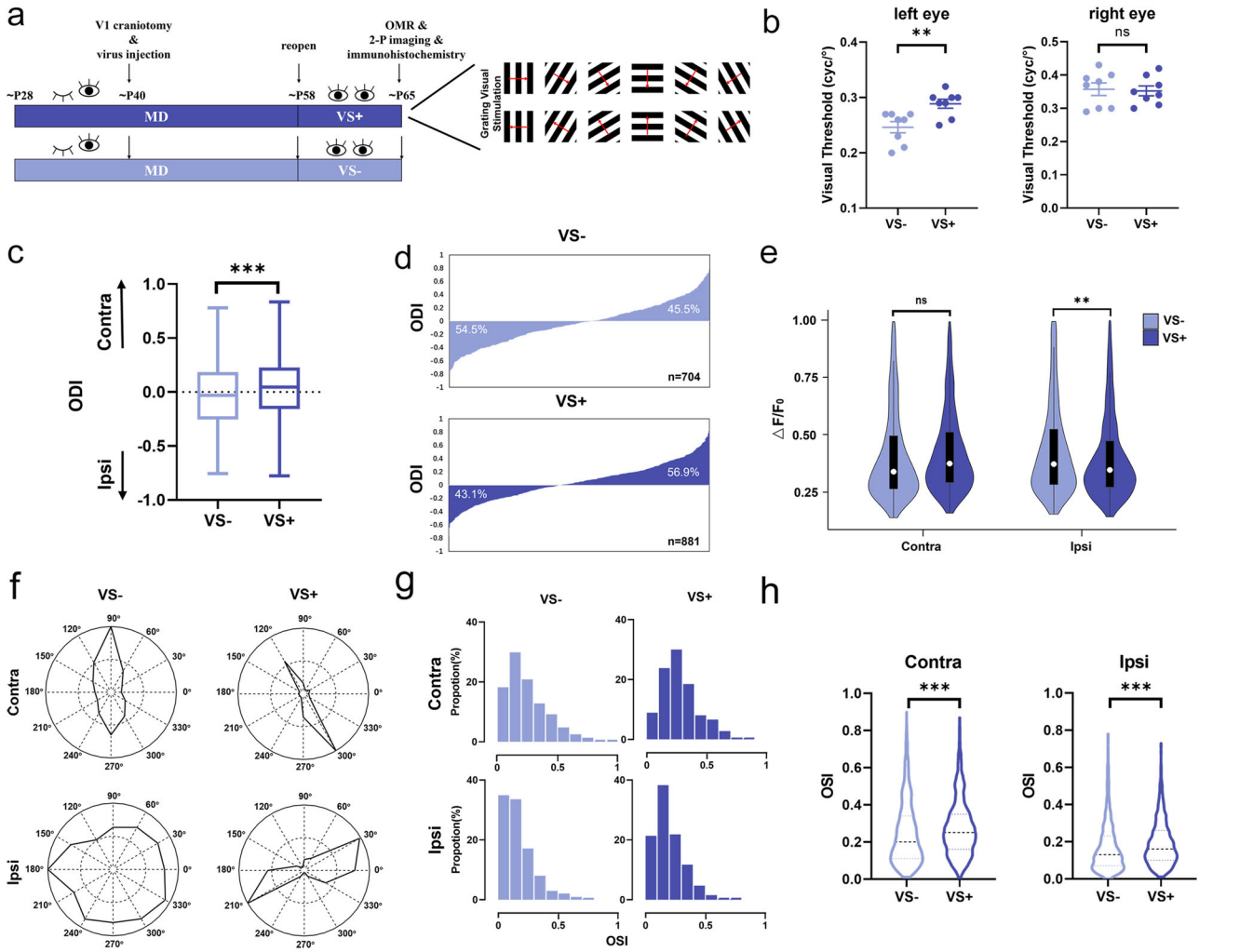

Fig. 4 | Visual stimulation training reactivates ocular dominance plasticity and promotes vision recovery in adult amblyopic mice. a Left panel: Experimental timeline. Mice underwent 30 days of MD via lid suturing of the left eye from P28 to P58. Cranial window surgery and/or virus injection surgery were performed two to three weeks before reopening the deprived eye. Two recovery groups with either grating visual stimulation training (VS+, 1 h/day, 7 days) from P58-P65 or without visual stimulation (VS−) were recorded at P65. Right panel: Sinusoidal black and white gratings used for visual stimulation training, with a spatial frequency of 0.05 cycles/degree and a drift speed of 1 Hz, moving in 12 different directions. **b** Visual acuity thresholds of the left ($t = 3.267$, $p = 0.006$) and right ($t = 0.208$, $p = 0.838$) eyes of the mice in the VS− and VS+ groups ($n = 8$ mice/group). **c** Comparisons of the ODIs of V1 excitatory neurons. VS−: $n = 740$ neurons; VS+: $n = 881$ neurons. $t = 5268$, $p < 0.001$. **d** Distributions of the ODI and the percentage of excitatory neurons whose ODI is above (contralateral bias) or below (ipsilateral bias) zero. **e** Violin plots and overlaid box plots of the response amplitude of V1 excitatory neurons. Contra: $t = 1.537$, $p = 0.125$; Ipsi: $t = 2.706$, $p = 0.007$. **f** Representative polar plots of the responses to drifting gratings of the contralateral or ipsilateral eye from an excitatory neuron in each group. **g** Population distributions of the OSI of V1 excitatory neurons. **h** Comparisons of the OSI of V1 excitatory neurons. Contra: $t = 4.853$, $p < 0.001$; Ipsi: $t = 4.309$, $p < 0.001$. For all figures: two-tailed independent samples t-tests were used to compare the VS− and VS+ groups; $^{**}p < 0.01$; $^{***}p < 0.001$; ns no significant difference. The error bars indicate the SEMs.

dominance plasticity in mice. Hosang et al.[20] reported that long-term training using a visual water task increases the visual acuity of MD-treated mice. Although opinions differ concerning whether the recovery of neuronal response and visual functions are specific to the particular visual stimuli presented during locomotion or visual stimulation alone[52], the improved visual function of the amblyopic eye following visual perceptual learning has also been observed in amblyopic patients[14,71], indicating homeostatic plasticity mechanisms that operating in the amblyopic visual system and opening up a new way to therapeutic approaches for the treatment of adult amblyopia. However, in the present study, even after visual stimulation treatment, neither the visual acuity threshold nor the ODI or OSI of excitatory neurons in V1 recovered to the levels in normal mice. We speculate that our mice were still in the critical period of visual development when MD was conducted, and long-term MD caused irreversible damage to their visual development, especially additional deficits in higher visual areas that may not be uniformly inherited from V1[46,72].

Our results show that under the influence of long-term MD and visual stimulation training, the ocular dominance shift in amblyopic mice is achieved by a change in the nondeprived-eye input (see Figs. 1g and 4e). This finding concurs with an earlier study in which adult (more than P120) mice were monocularly deprived for 7 days; in these animals, the observed ocular dominance shift was mediated by an increase in nondeprived-eye responses[73]. Indeed, the varying eye-specific effects of ocular dominance plasticity differ between the critical period and adulthood. During the critical period, a weakening of deprived-eye input is characteristic of the juvenile form of ocular dominance plasticity[39,74], whereas in adult animals, strengthening of the nondeprived-eye response becomes dominant[74,75], although some studies also find evidence for additional deprived-eye depression[20,76,77]. In our study, the ocular dominance shift was attained by an increase in the response from the nondeprived eye after 30 days of MD and by a decrease in response from the same eye after 7 days of visual stimulation training, thus resembling adulthood plasticity. In addition, our results

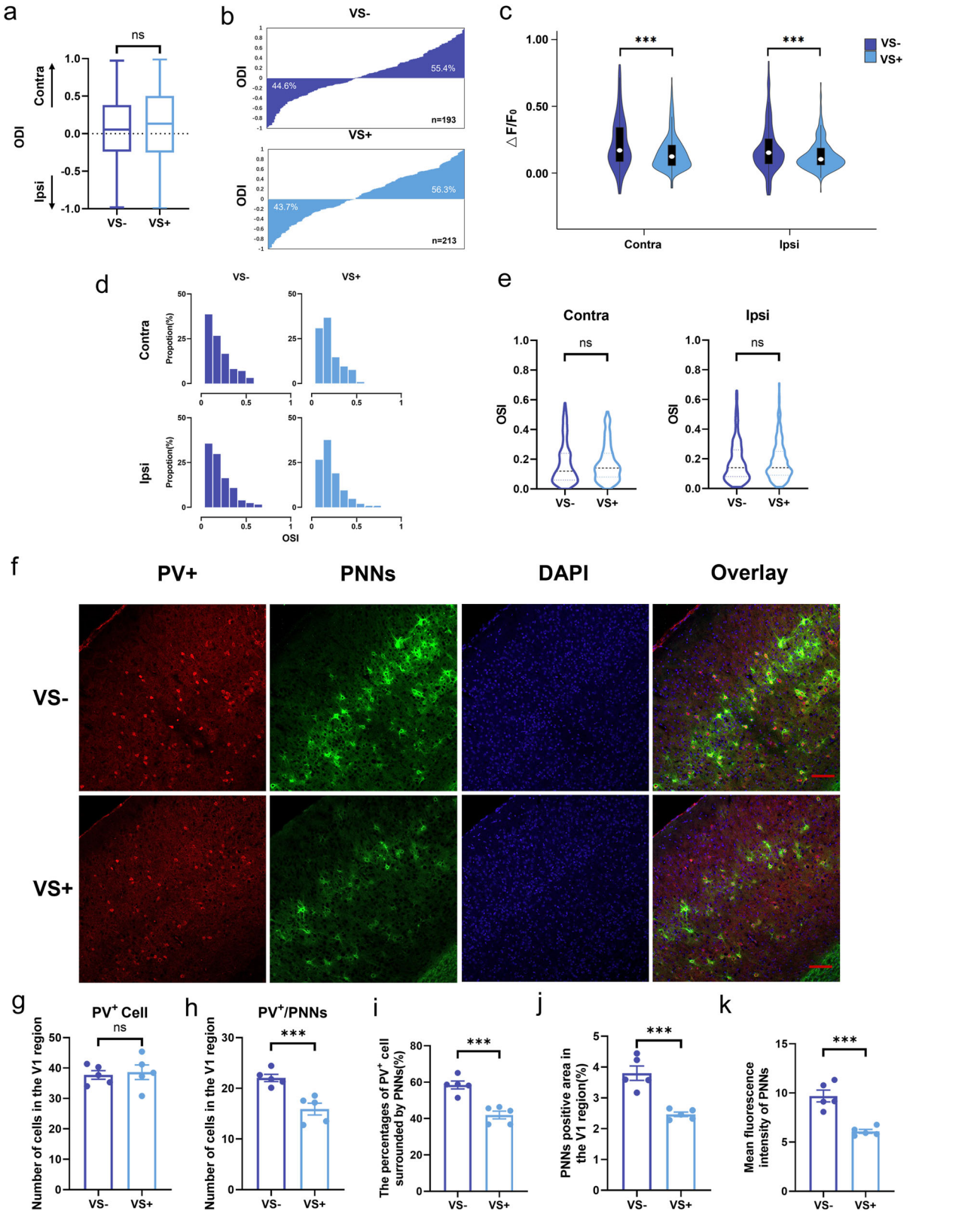

Fig. 5 | Visual stimulation training decreases the response of PV$^+$ interneurons and the density of PNNs surrounding PV$^+$ interneurons in adult amblyopic mice. **a** Comparisons of the ODI of V1 PV$^+$ interneurons. VS-: $n = 193$ neurons; VS+: $n = 213$ neurons. $t = 0.707$, $p = 0.480$. **b** Distributions of the ODI and the percentage of PV$^+$ interneurons whose ODI is above (contralateral bias) or below (ipsilateral bias) zero. **c** Violin plots and overlaid box plots of the response amplitude of V1 PV$^+$ interneurons. Contra: $t = 4.789$, $p < 0.001$; Ipsi: $t = 3.387$, $p < 0.001$. **d** Population distributions of the OSI of V1 PV$^+$ interneurons. **e** Comparisons of the OSIs of V1 PV$^+$ interneurons. Contra: $t = 0.340$, $p = 0.734$; Ipsi: $t = 0.318$, $p = 0.350$. **f** Representative fluorescence photomicrographs of coronal V1 sections from one animal in each group ($n = 5$ mice/group). Scale bar, 50 μm. **g** Density of PV$^+$ interneurons. $t = 0.301$, $p = 0.764$. **h** Density of PV$^+$ interneurons surrounded by PNNs. $t = 5.604$, $p < 0.001$. **i** Percentages of PV$^+$ interneurons surrounded by PNNs. $t = 7.016$, $p < 0.001$. **j** PNNs-stained area. $t = 5.455$, $p < 0.001$. **k** The mean intensity of PNNs fluorescence. $t = 5.734$, $p < 0.001$. For all figures: two-tailed independent samples t-tests were used to compare the VS− and VS+ groups; ***$p < 0.001$; ns no significant difference. The error bars indicate the SEMs.

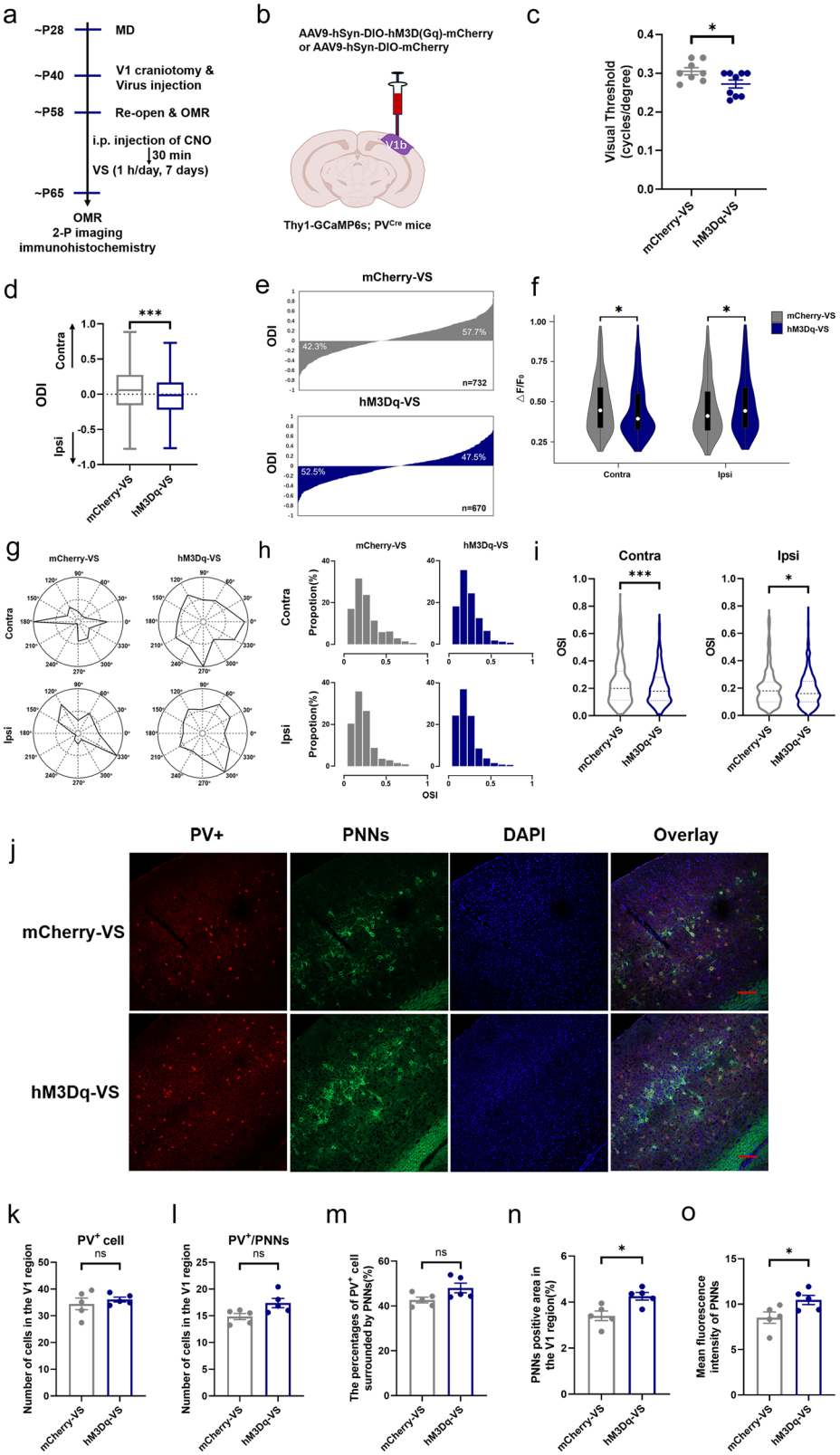

Fig. 6 | Activation of PV$^+$ interneurons offsets the vision-promoting effects of visual stimulation training in adult amblyopic mice. a Schematic of the experimental design. VS visual stimulation. **b** Illustration of the specific infection of V1 PV$^+$ interneurons with hM3Dq-mCherry or mCherry. **c** Comparisons of visual acuity thresholds after 7 days of CNO injection accompanied by visual stimulation training ($n = 8$ mice/group). $t = 2.509$, $p = 0.025$. **d** Comparisons of the ODI of V1 excitatory neurons. mCherry-VS: $n = 732$ neurons; hM3Dq-VS: $n = 670$ neurons. $t = 4.201$, $p < 0.001$. **e** Distributions of the ODI of V1 excitatory neurons and the percentage of excitatory neurons whose ODI is above (contralateral bias) or below (ipsilateral bias) zero. **f** Violin plots and overlaid box plots of the responses of V1 excitatory neurons. Contra: $t = 2.548$, $p = 0.011$; Ipsi: $t = 2.121$, $p = 0.034$. **g** Representative polar plots of the responses to drifting gratings of the contralateral or ipsilateral eye from an excitatory neuron of each group. **h** Population distributions of the OSI of V1 excitatory neurons. **i** Comparisons of the OSI of V1 excitatory neurons. Contra: $t = 3.696$, $p < 0.001$; Ipsi: $t = 1.989$, $p = 0.047$. **j** Representative fluorescence photomicrographs of coronal V1 sections from one animal in each group ($n = 5$ mice/group). Scale bar, 50 μm. **k** Density of PV$^+$ interneurons. $t = 0.687$, $p = 0.511$. **l** Density of PV$^+$ interneurons surrounded by PNNs. $t = 2.247$, $p = 0.055$. **m** Percentages of PV$^+$ interneurons surrounded by PNNs. $t = 2.142$, $p = 0.065$. **n** PNNs-stained area. $t = 3.214$, $p = 0.012$. **o** The mean intensity of PNNs fluorescence. $t = 2.430$, $p = 0.041$. For all figures: two-tailed independent samples t-tests were used to compare the mCherry-VS and hM3Dq-VS groups; $^*p < 0.05$; $^{***}p < 0.001$; ns no significant difference. The error bars indicate the SEMs.

showed a significant reduction in orientation selectivity of both the responses of the deprived-eye and nondeprived-eye following long-term MD and a significant increase following visual training. This finding is partially consistent with the conclusion reported by Craddock et al.[46], who documented that the OSI for the contralateral eye in V1b of young adult mice (2-3 months) decreased after 2 weeks of MD. The difference is that they also observed an increase in the OSI of responses through the ipsilateral eye (although it failed to reach significance), which we think may be due to differences in the age groups and durations of MD in mice. In fact, given that amblyopia harms the development of the binocular visual system and the interactions between signals from two eyes, many studies have indicated visual function deficits (contrast sensitivity, spatial integration, global

motion, etc.) in the fellow eye even though it exhibits normal visual acuity[78]. Therefore, we speculate that amblyopia caused by early-onset, long-term MD may exhibit a reduction of the OSI of responses through both the deprived and nondeprived eyes.

Our findings focus on PV^+ interneurons as the initial locus underlying the neuronal changes in amblyopia and the effects of visual stimulation training, which adjusts synaptic inhibition to excitatory neurons and controls cortical plasticity[28]. This E/I balance mechanism identified in our work unifies the findings of previous studies in which PV^+ interneurons are believed to be the primary source of inhibition in V1 and inhibitory and excitatory inputs to individual neurons in V1 are normally balanced; however, MD causes their relative strengths to diverge[28,31,79,80]. A reduction in PV^+ interneuron activities and disinhibition of upper-layer excitatory neurons are involved in the initial stages of cortical plasticity in adolescence through a loss of the excitatory drive to PV^+ interneurons[28,32,81]. In the present study, the chemogenetic reduction in PV^+ interneuron responses enhanced ocular dominance plasticity, reduced the density of PNNs and promoted vision recovery from amblyopia. Conversely, the chemogenetic activation of PV^+ interneurons during visual stimulation training prevented the recovery of ocular dominance plasticity, increased the density of PNNs and blocked the vision-promoting effects of visual stimulation training. Furthermore, it is worth determining the role of PV-mediated mechanisms and/or PNNs in V1 plasticity of amblyopic mice, for example, a targeted reduction in the contribution of fast-spiking inhibitory interneurons through disruption of the GAD65 gene in mice, attenuation of the release of GABA neurotransmitter[25] or enzymatic removal of PNNs through intracortical administration of proteases to observe the capacity for plasticity in the visual system[82], during amblyopia treatment with physiological or behavioral effects. In a word, these findings define the microcircuit changes initiating competitive plasticity in the primary visual cortex and imply that the restoration of inputs to excitatory neurons by PV^+ interneuron-specific disinhibition is a key step in the progression of adult cortical plasticity.

PNNs are molecular aggregations that primarily surround PV^+ interneurons and exhibit properties congruent with those of plasticity inhibitors for experience-dependent plasticity in the visual cortex[33]. We observed that visual stimulation training significantly reduces the density of PNNs and the proportion of PV^+ interneurons surrounded by PNNs but does not alter the number of PV^+ interneurons in V1. These results are consistent with those of previous studies revealing a dark rearing-induced reduction in PNNs[39,49], suggesting that the maturity of PNNs is inhibitory for experience-dependent plasticity and that the degradation of PNNs reactivates cortical plasticity. Although this study focused mainly on PV^+ interneurons and PNNs, amblyopia may have an impact on non-PV^+ interneurons. For example, PV^+ interneurons can be inhibited by SST interneurons and VIP interneurons preferentially inhibit SST interneurons[83–85]. Further studies are required to determine how amblyopia and visual stimulation treatment affect the responses and interactions of excitatory neurons and specific classes of interneurons.

In summary, using monocular deprivation in juvenile mice to model amblyopia, we demonstrated an E/I imbalance between excitatory neurons and PV^+ interneurons in the primary visual cortex of amblyopic mice, that could be reversed by visual stimulation treatment to achieve better vision recovery. Our results reveal the neuronal interactions underlying amblyopia and the neural plasticity-based mechanism for visual stimulation-mediated functional recovery from adult amblyopia, providing evidence for therapeutic applications that rely on reactivating adult cortical plasticity.

Materials and methods

Ethics statement

All experiments were carried out strictly according to the Animal Research: Reporting of In Vivo Experiments (ARRIVE) guidelines 2.0[86], the Guide for the Care and Use of Laboratory Animals, and the Association for Research in Vision and Ophthalmology (ARVO) statement on animal use. All experimental protocols were approved by the Institutional Animal Care and Use Committee of the Laboratory Animal Center, Zhongshan School of Medicine, Sun Yat-sen University (approval no. 2019-1210; approval date: March 28, 2019). We have complied with all relevant ethical regulations for animal use. Mice were bred in-house with constant temperature, humidity, and a 12-h light/dark cycle. Food and water were provided ad libitum during the entire experimental period.

Experimental animals

C57BL/6 mice of both sexes were used in the visual function test ($n = 39$) and immunohistochemistry ($n = 35$). Thy1-GCaMP6s transgenic mice (C57BL/6J-Tg (Thy1-GCaMP6s) GP4.3Dkim/J, JAX 024275, The Jackson Laboratory), which express the green fluorescent calcium indicator GCaMP6s in subsets of excitatory neurons in the brain ($n = 16$), and PV^{Cre} mice (B6.129P2-Pvalb$^{tm1(cre)Arbr/J}$, JAX 017320, The Jackson Laboratory), which express Cre recombinase in parvalbumin-expressing neurons in the brain ($n = 16$), were used for in vivo two-photon calcium imaging (2-P imaging). Offspring of Thy1-GCaMP6s transgenic mice crossed with PV^{Cre} mice (Thy1-GCaMP6s; PV^{Cre} mice) were used for the visual function test ($n = 40$) and 2-P imaging ($n = 24$) with chemogenetics (CNO-hM4Di/hM3Dq/mCherry). Both male and female offspring were used. Litter mates were randomly allocated to different experimental groups.

Generation and phenotyping of the mouse line

For Thy1-GCaMP6s, 5′-CAT CAG TGC AGC AGA GCT TC-3′ and 5′-CAG CGT ATC CAC ATA GCG TA-3′ were designed as forward and reverse primers, respectively, for the mutant. The predicted band was 248 bp for the mutant GCaMP6s mouse. For PV^{Cre} mouse, the following pairs of primers were used to detect the presence of Cre recombinase: 5′-AAA TGC TTC TGT CCG TTT GC-3′ and 5′-ATG TTT AGC TGG CCC AAA TG -3′. A 163-bq band was predicted for the mutant Cre mouse. Thy1-GCaMP6s; PV^{Cre} mice were generated by crossing the two mouse lines mentioned above. Offspring were genotyped for the expression of Cre and GCaMP6s.

A 0.5 cm piece of the tail was removed from each mouse using sterilized scissors. The tail pieces were processed using a mouse tail rapid genotype identification kit (Beyotime, Shanghai, China). The PCR amplifier (Bio-Rad, Hercules, CA, USA) settings were as follows: 94 °C for 3 min, 94 °C for 30 s, 55 °C for 30 s, 72 °C for 30 s, and 72 °C for 10 min. The cycle was repeated 25 times and then samples were stored at 4 °C. Electrophoresis was run in a 2% agarose gel.

Monocular deprivation

The mice were subjected to MD via lid suturing at P28 under deep anesthesia with an intraperitoneal injection of Avertin (250 mg/kg). MD was performed on the left eye according to published protocols[18,64]. The lid margins of the left eye were trimmed, and the upper and lower eyelids were sutured closed using two mattress sutures (6–0 silk, Alcon). Tobramycin eye ointment was applied to prevent infection. Mice were returned to their home cages after waking up. All mice were monocularly deprived for 30 days and checked daily to ensure that the eye remained closed. An ophthalmoscope was used to verify the clarity of the optic media after reopening the eye. Mice with early eyelid dehiscence and opaque optic media were not used in subsequent experiments.

Implantation of the cranial window and intracranial virus injection

Two to three weeks before reopening the deprived eye, cranial window surgery and/or virus injection surgery were performed. Based on previous studies, a modified surgery was performed[87]. Mice were given dexamethasone (5 mg/kg i.p.) to prevent cerebral edema six hours before the surgery and placed on a heating pad to maintain body temperature at 37 °C with the eyes covered by protective ophthalmic cream during the surgery. The surgical area was disinfected three times with 70% ethanol. During surgery, mice were deeply anesthetized with an intraperitoneal injection of Avertin (250 mg/kg). The skin was removed with a midline scalp incision and the edges of the incision were attached to the skull with tissue adhesive (Vetbond, 3 M). The periosteum tissue over the skull surface was removed with toothed forceps. The right-side V1 region was identified based on

stereotactic coordinates (2.7 mm lateral to the midline and 3.5 mm posterior to the bregma) and was marked. A head holder consisting of a metal ring with two bars was attached to the mouse skull with glue (Loctite 495, Henkel, Dusseldorf, Germany), and the center of the head holder was placed on the marked area to restrain the head. When the glue dried, a dental drill was applied to thin the marked skull, and the round skull area of approximately 3 × 3 mm was then peeled off with microforceps. The dura over the exposed cortex was partially removed to avoid bleeding and the formation of neovascular membranes, allowing the observation area to be more clearly visualized.

To perform the intracranial virus injection, the mice were placed in a stereotaxic instrument, and the injection was performed via a micropipette connected to a Nanoliter Injector (Nanoject III) at a slow flow rate of 30 nl/min to avoid potential damage to local brain tissue. Then, 300 nl of virus (virus titer of 10^{12} genomes/ml) was injected into the V1b area of the right hemisphere at a depth of 200–300 μm. The V1b was defined using stereotaxic coordinates 3.2–3.5 mm lateral from lambda and 2.5–3.0 mm behind the bregma. After the injection, a small 3 × 3 mm round glass glued to a 5 × 5 mm round cover-glass using biological glue (Kwik-Sil Adhesive, WPI) was placed on the exposed cortex and the edges of the glass were sealed to the skull with glue. The mouse was then placed in a heated recovery chamber before being returned to the home cage. A subcutaneous injection comprising Tolfedine (4 mg/kg), Butomidor (2 mg/kg), and Baytril (5 mg/kg) was administered every 3 days to prevent inflammation, pain, and infection. Cre-dependent rAAV-Ef1α-DIO-Gcamp6f (BrainVTA, China) was used to drive Gcamp6f expression in the PV^{+} interneurons of PV^{Cre} mice. Cre-dependent AAV9-hSyn-DIO-hM3D(Gq)-mCherry and AAV9-hSyn-DIO-hM4D(Gi)-mCherry (BrainVTA, China) were used to drive hM3Dq and hM4Di expression, respectively, in PV^{+} interneurons of Thy1-GCaMP6s; PV^{Cre} mice, with AAV9-hSyn-DIO-mCherry also used as a control vector. The specificity and efficiency of the DREADD system were tested and are shown in Supplementary Fig. 4.

Measurement of optomotor response (OMR) and visual stimulation training

The OMR is a reflex used to assess visual functions[88,89]. Stimulus-correlated head movements are quantified to determine visual acuity thresholds. In this study, the OMRs of awake, behaving mice to visual stimuli in the form of a moving grating were measured using the PhenoSys qOMR (quantitative OMR), a unique system that automatically measures OMRs with a virtual stimulation sphere that continuously aligns with the animal's head position based on real-time head tracking[45,90]. Briefly, mice were positioned on a platform and presented with sinusoidal gratings at different spatial frequencies of 0.05, 0.1, 0.2, 0.3, 0.4, and 0.5 cycles/degree with a stimulus speed of 12 degrees/second on 4 LCD screens that surrounded the test animal. Sinusoidal gratings were presented for 2 min per spatial frequency, and there was a gray-out pause for 10 s between sinusoidal gratings of different spatial frequencies to help the animal relax and increase attention to the next stimulus. Stimuli presentation was controlled using OmrStudio software to produce a virtual cylinder that maintained a constant distance between the grating and the horizontal visual field of the tested animal located at the center of the apparatus (see Fig. 1b). To measure the elicited OMRs, the head movements of the unrestrained tested mice were video recorded by a camera placed above and analyzed by an algorithm that tracks the position of each mouse's head. These data were used to automatically readjust the presentation of the stimuli to changing head positions to keep the size of the grating constant. OMR measurements were obtained objectively using an automated approach during offline analysis and did not involve subjective grading or input from a human observer. OMR tracking behavior was quantified as the ratio of the total amount of time that the animal's head moved in the stimulus direction to the amount of time that the head moved against the stimulus direction ($T_{correct}/T_{incorrect}$). Each animal was measured under each spatial frequency 3 to 5 times. The absolute values of the $T_{correct}/T_{incorrect}$ of different trials and different spatial frequencies for each mouse were collected, resulting in a curve that peaked somewhere in the range of 0.2 cycles/degree. Separate analysis of the two different rotating directions of the stimulus was set to differentiate between the left and right eye reactions, with the result for the clockwise motion of the stimulus attributed to the left eye and the result for the counterclockwise motion attributed to the right eye. The visual acuity threshold was defined as the spatial frequency corresponding to 50% of the maximum optomotor response.

Visual stimulation training was also carried out in the OMR arena binocularly. After 30 days of MD and reopening of the left eye, each amblyopic mouse was placed into the OMR arena for one hour of binocular visual stimulation training during daylight for seven consecutive days. The mouse was positioned on the central platform and the surrounding four display screens showed sinusoidal black and white gratings with a spatial frequency of 0.05 cycles/degree and a drift speed of 1 Hz, moving in 12 different directions, which matched the spatiotemporal frequency response of the mouse. Before the visual stimulation training officially began, each mouse was given 10 min to adapt. The one-hour training was evenly divided into four blocks. Between blocks, each mouse could take a short break to avoid fatigue.

Two-photon calcium imaging and analysis

Procedures for two-photon calcium imaging were based on the previous literature[66,91]. Calcium imaging was obtained using a two-photon microscopy (FVMPE-RS multiphoton laser scanning microscope; Olympus, Tokyo, Japan) with the laser tuned to 920 nm and the power maintained in the range of 25–35 MW (25 × objective and numerical aperture of 1.05, immersed in artificial cerebrospinal fluid). A custom-built light protective cone was fitted around the objective to prevent extraneous illumination. Images were acquired over a field of view of 509 × 509 μm located in the V1b area at 15 fps (resonant scan). We positioned the field of view 1 mm anterior to the rear of the cranial window aligned horizontally to the midline of the cranial window. All imaging was performed at a depth of 200–300 μm below the pia as measured from the center of the field of view in awake, head-fixed mice held stationary in an aluminum plate. Visual stimuli generated by the MATLAB (MathWorks) toolbox, Psychtoolbox[92] were presented on an LCD monitor on the left or right side 25 cm from the mouse's eye. Visual stimuli consisting of drifting, sinusoidal gratings with a spatial frequency of 0.05 cycles/degree and moving 1 cycle/second were presented in 12 directions of motion in 30° steps to elicit calcium responses. The stimulus in each direction was repeated 5 times in a pseudorandom order. Visual stimuli were presented for 4 s each, with a gray screen of 4 s presented between visual stimuli. Mice were anesthetized with 1% isoflurane, placed below the objective, and allowed to habituate for 30 min before imaging. During imaging, mice were presented with visual stimuli shown to one eye at a time by placing an opaque eye block in front of the opposing eye to temporarily occlude vision. The eye stimulated first (left or right) was randomized between animals and recordings. After each imaging session, mice were placed in a heated chamber until they fully recovered and then returned to their home cage.

The two-photon calcium imaging analysis pipeline, Suite2P (https://github.com/MouseLand/suite2p) was used to register and detect cells in the recorded data (suite2p, version 0.8.0, RRID: SCR_016434)[93]. All images collected from a single area at the same resolution and wavelength were registered via phase correlation to correct the effects of brain movement. Then, a set of spatial regions of interest (ROIs) were detected with positive weights for each pixel and distinguished as cell and noncell ROIs. Finally, the single fluorescence signal for each ROI, corrected by removing the neuropil contamination signal was extracted to represent the calcium fluorescence time course of the ROI (Supplementary Fig. 5). For calcium fluorescence analysis, we used custom-written MATLAB scripts (MathWorks). The visually evoked response of each cell was computed as changes in fluorescence relative to the baseline, namely, $\Delta F/F_0 = (F-F_0)/F_0$, where F_0 was the average fluorescence when there was no stimulus presented (defined as the last 25% of time before the stimulus presentation; 1 s in total), and F was the average fluorescence when the stimulus was presented (defined as the last

75% of time when the stimulus was presented and 25% of time after the end of the stimulus; 4 s in total). A visually responsive neuron was identified as one in which the F of a neuron was more than 2 times the standard deviation of F_0 in at least one orientation. The $\Delta F/F_0$ of each visually responsive neuron was used to calculate the ODI and OSI. The ODI of each visually responsive neuron was calculated as

$$\mathrm{ODI} = \frac{C - I}{C + I}$$

where C and I represent the maximum response magnitudes of the contralateral and ipsilateral eyes, respectively.

We calculated the OSI by vector averaging as OSI = 1 – circular variance (CV)[94], with

$$\mathrm{CV} = \left| \frac{\sum_k R(\theta_k) \exp(2i\theta_k)}{\sum_k R(\theta_k)} \right|$$

where θ_k is the orientation of a visual stimulus and $R(\theta_k)$ is the response to that stimulus.

Tissue preparation, immunofluorescence staining, microscopy and analysis

C57BL/6 mice were anesthetized with intraperitoneal injections of pentobarbital sodium and perfused transcardially with normal saline followed by 4% paraformaldehyde (PFA). The brains were carefully dissected, fixed in 4% PFA overnight, dehydrated, embedded in TissueTek OCT compound, frozen in isopentane, and cut into coronal sections at 14 μm for immunofluorescence staining. The brain samples were prepared for different groups of mice ($n = 5$ mice for each group).

The frozen sections were air-dried for at least 30 min, rehydrated with 0.1 M phosphate-buffered saline (PBS) for 10 min, incubated in a PBS solution containing 0.03% Triton X-100 for half an hour, and then blocked with 10% normal goat serum for 1 h at RT. To label PV^+ interneurons and PNNs, the primary marker, a monoclonal mouse antibody against parvalbumin (1:2000; Sigma P3088) was applied along with Wisteria floribunda agglutinin (WFA; 1: 100; Sigma–Aldrich) in PBS, and then incubated overnight at 4 °C. Sections were rinsed with PBS three times (5 minutes each) and then incubated with secondary antibodies, Alexa Fluor 555 goat anti-mouse IgG (XYM-Bioss-0296G555 1:500; Bioss Antibodies, China) and Alexa-647 streptavidin conjugate (1:500; Asbio, China) diluted in PBS for 1 h at RT in the dark. After another three washes with PBS, the coverslip slides were treated with an antifade reagent with DAPI (F6057, Sigma–Aldrich, USA).

Sections were viewed using a confocal microscope (LSM 780 or LSM 980, Zeiss, Germany). A 10× objective lens (FLUAR, NA = 0.5, WD = 2 mm) was used for imaging. Typically, three sections of the contralateral (right side) V1 region were captured per animal. All images were analyzed using Fiji/ImageJ software. We estimated the density of PV^+ interneurons and PNNs, and the ratio of PV^+ interneurons surrounded by PNNs (PV^+/PNNs). A 500 × 500 mm ROI was analyzed per image, positioned in layers II-V of V1. PV^+ interneurons and PNNs were counted separately per image. Then, both images were superimposed, and cells showing colocalization were counted manually. The percentages of PV^+ interneurons surrounded by PNNs (% colocalization) were calculated as follows:

$$\%\mathrm{colocalization} = \left(\frac{\text{cells with colocalization of } PV^+ \text{ and PNNs}}{\text{total } PV^+ \text{ count}} \right) \times 100\%$$

The densities of cells immunoreactive for PV^+ interneurons and PV^+ interneurons surrounded by PNNs, as well as the percentages of colocalization were determined for each group, and the means ± SEMs were calculated. The mean intensity of the fluorescence of WFA staining for PNNs and the percentage of area covered by PNNs were calculated as follows: after transforming the image to 8-bit depth, the background was subtracted (rolling value = 30) to obtain the mean intensity. The percentage of area covered by PNNs was then calculated by applying a predetermined threshold (value = 5) and measuring the binarized area with respect to the total area of the image.

Statistics and reproducibility

Data are reported as the means ± standard deviations (SDs) unless otherwise noted. Statistical analyses were performed with Prism 8.0 (GraphPad, San Diego, CA, USA) and IBM SPSS version 25 (IBM, Armonk, NY, USA). Each neuron recorded was considered an independent sample for analysis of ODI, $\Delta F/F_0$ and OSI. Mean values were calculated on a per-animal basis for analysis of immunofluorescence staining. The normality of distribution was tested. Two-tailed independent sample tests were used to assess the differences between two groups. All the data were considered statistically significant at $p < 0.05$. Specific statistical tests for each data set and p-values can be found within the corresponding figure legends.

Reporting summary

Further information on research design is available in the Nature Portfolio Reporting Summary linked to this article.

Data availability

The source data used to generate the main figures are provided in the Supplementary Data. All other relevant raw data are available from the corresponding author upon reasonable request.

Received: 16 May 2024; Accepted: 19 November 2024;
Published online: 25 November 2024

References

1. Baroncelli, L. & Lunghi, C. Neuroplasticity of the visual cortex: In sickness and in health. *Exp. Neurol.* **335**, 113515 (2021).
2. Berry, K. P. & Nedivi, E. Experience-dependent structural plasticity in the visual system. *Annu. Rev. Vis. Sci.* **2**, 17–35 (2016).
3. Espinosa, J. S. & Stryker, M. P. Development and plasticity of the primary visual cortex. *Neuron* **75**, 230–249 (2012).
4. Cruz, O. A. et al. Amblyopia preferred practice pattern. *Ophthalmology* **130**, P136–P178 (2023).
5. Fu, Z. et al. Global prevalence of amblyopia and disease burden projections through 2040: A systematic review and meta-analysis. *Br. J. Ophthalmol.* **104**, 1164–1170 (2020).
6. Birch, E. E. et al. Self-perception in children aged 3 to 7 years with amblyopia and its association with deficits in vision and fine motor skills. *JAMA Ophthalmol.* **137**, 499–506 (2019).
7. Birch, E. E. et al. Self-perception of school-aged children with amblyopia and its association with reading speed and motor skills. *JAMA Ophthalmol.* **137**, 167–174 (2019).
8. Carlton, J. & Kaltenthaler, E. Amblyopia and quality of life: A systematic review. *Eye* **25**, 403–413 (2011).
9. Epelbaum, M., Milleret, C., Buisseret, P. & Dufier, J. L. The sensitive period for strabismic amblyopia in humans. *Ophthalmology* **100**, 323–327 (1993).
10. Gao, T. Y. et al. Effectiveness of a binocular video game vs placebo video game for improving visual functions in older children, teenagers, and adults with amblyopia: A randomized clinical trial. *JAMA Ophthalmol.* **136**, 172–181 (2018).
11. Bossi, M. et al. Binocular therapy for childhood amblyopia improves vision without breaking interocular suppression. *Invest. Ophthalmol. Vis. Sci.* **58**, 3031–3043 (2017).
12. Liu, Z. et al. A new dichoptic training strategy leads to better cooperation between the two eyes in amblyopia. *Front. Neurosci.* **14**, 593119 (2020).
13. Gu, L. et al. Effects of monocular perceptual learning on binocular visual processing in adolescent and adult amblyopia. *iScience* **23**, 100875 (2020).

14. Li, J. et al. Dichoptic training enables the adult amblyopic brain to learn. *Curr. Biol. CB* **23**, R308–R309 (2013).
15. Pineles, S. L. et al. Binocular treatment of amblyopia: A report by the american academy of ophthalmology. *Ophthalmology* **127**, 261–272 (2020).
16. Kelly, K. R. et al. Binocular ipad game vs patching for treatment of amblyopia in children: A randomized clinical trial. *JAMA Ophthalmol.* **134**, 1402–1408 (2016).
17. Holmes, J. M. et al. Effect of a binocular ipad game vs part-time patching in children aged 5 to 12 years with amblyopia: A randomized clinical trial. *JAMA Ophthalmol.* **134**, 1391–1400 (2016).
18. Gordon, J. A. & Stryker, M. P. Experience-dependent plasticity of binocular responses in the primary visual cortex of the mouse. *J. Neurosci.* **16**, 3274–3286 (1996).
19. Hubel, D. H. & Wiesel, T. N. The period of susceptibility to the physiological effects of unilateral eye closure in kittens. *J. Physiol.* **206**, 419–436 (1970).
20. Hosang, L., Yusifov, R. & Löwel, S. Long-term visual training increases visual acuity and long-term monocular deprivation promotes ocular dominance plasticity in adult standard cage-raised mice. *Eneuro* **5**, ENEURO.0289–0217.2017 (2018).
21. Matthies, U., Balog, J. & Lehmann, K. Temporally coherent visual stimuli boost ocular dominance plasticity. *J. Neurosci.* **33**, 11774–11778 (2013).
22. Mitchell, D. E. & Sengpiel, F. Neural mechanisms of recovery following early visual deprivation. *Philos. Trans. R. Soc. Lond. Ser. B Biol. Sci.* **364**, 383–398 (2009).
23. Fang, Q. et al. Balanced enhancements of synaptic excitation and inhibition underlie developmental maturation of receptive fields in the mouse visual cortex. *J. Neurosci.* **41**, 10065–10079 (2021).
24. Ma, W.-p, Li, Y.-t & Tao, H. W. Downregulation of cortical inhibition mediates ocular dominance plasticity during the critical period. *J. Neurosci.* **33**, 11276–11280 (2013).
25. Hensch, T. K. et al. Local gaba circuit control of experience-dependent plasticity in developing visual cortex. *Science* **282**, 1504–1508 (1998).
26. Fagiolini, M. & Hensch, T. K. Inhibitory threshold for critical-period activation in primary visual cortex. *Nature* **404**, 183–186 (2000).
27. Takesian, A. E. & Hensch, T. K. Balancing plasticity/stability across brain development. *Prog. Brain Res.* **207**, https://doi.org/10.1016/B978-0-444-63327-9.00001-1 (2013).
28. Kuhlman, S. J. et al. A disinhibitory microcircuit initiates critical-period plasticity in the visual cortex. *Nature* **501**, 543–546 (2013).
29. Hensch, T. K. & Stryker, M. P. Columnar architecture sculpted by gaba circuits in developing cat visual cortex. *Science* **303**, 1678–1681 (2004).
30. Morishita, H., Cabungcal, J.-H., Chen, Y., Do, K. Q. & Hensch, T. K. Prolonged period of cortical plasticity upon redox dysregulation in fast-spiking interneurons. *Biol. Psychiatry* **78**, 396–402 (2015).
31. Sun, Y. et al. Neuregulin-1/erbb4 signaling regulates visual cortical plasticity. *Neuron* **92**, 160–173 (2016).
32. Grieco, S. F. et al. Subanesthetic ketamine reactivates adult cortical plasticity to restore vision from amblyopia. *Curr. Biol.* **30**, 3591-+ (2020).
33. Reichelt, A. C., Hare, D. J., Bussey, T. J. & Saksida, L. M. Perineuronal nets: Plasticity, protection, and therapeutic potential. *Trends Neurosci.* **42**, 458–470 (2019).
34. Domínguez, S. et al. Maturation of pnn and erbb4 signaling in area ca2 during adolescence underlies the emergence of pv interneuron plasticity and social memory. *Cell Rep.* **29**, https://doi.org/10.1016/j.celrep.2019.09.044 (2019).
35. Lupori, L. et al. A comprehensive atlas of perineuronal net distribution and colocalization with parvalbumin in the adult mouse brain. *Cell Rep.* **42**, 112788 (2023).
36. Ye, Q. & Miao, Q.-L. Experience-dependent development of perineuronal nets and chondroitin sulfate proteoglycan receptors in mouse visual cortex. *Matrix Biol.* **32**, 352–363 (2013).
37. Pizzorusso, T. et al. Reactivation of ocular dominance plasticity in the adult visual cortex. *Science* **298**, 1248–1251 (2002).
38. Shmal, D., Mantero, G., Floss, T., Benfenati, F. & Maya-Vetencourt, J. F. Restoring vision in adult amblyopia by enhancing plasticity through deletion of the transcriptional repressor rest. *iScience* **27**, 109507 (2024).
39. Erchova, I., Vasalauskaite, A., Longo, V. & Sengpiel, F. Enhancement of visual cortex plasticity by dark exposure. *Philosophical Trans. R. Soc. Lond. Ser. B Biological Sci.* **372**, https://doi.org/10.1098/rstb.2016.0159 (2017).
40. Faulstich, M., van Alphen, A. M., Luo, C., du Lac, S. & De Zeeuw, C. I. Oculomotor plasticity during vestibular compensation does not depend on cerebellar ltd. *J. Neurophysiol.* **96**, 1187–1195 (2006).
41. Katoh, A., Kitazawa, H., Itohara, S. & Nagao, S. Dynamic characteristics and adaptability of mouse vestibulo-ocular and optokinetic response eye movements and the role of the flocculo-olivary system revealed by chemical lesions. *Proc. Natl Acad. Sci. USA* **95**, 7705–7710 (1998).
42. Liu, B.-H., Huberman, A. D. & Scanziani, M. Cortico-fugal output from visual cortex promotes plasticity of innate motor behaviour. *Nature* **538**, 383–387 (2016).
43. Prusky, G. T., Silver, B. D., Tschetter, W. W., Alam, N. M. & Douglas, R. M. Experience-dependent plasticity from eye opening enables lasting, visual cortex-dependent enhancement of motion vision. *J. Neurosci.* **28**, 9817–9827 (2008).
44. Tusa, R. J., Demer, J. L. & Herdman, S. J. Cortical areas involved in okn and vor in cats: Cortical lesions. *J. Neurosci.* **9**, 1163–1178 (1989).
45. Kretschmer, F., Kretschmer, V., Kunze, V. P. & Kretzberg, J. Omr-arena: Automated measurement and stimulation system to determine mouse visual thresholds based on optomotor responses. *PLoS ONE* **8**, e78058 (2013).
46. Craddock, R., Vasalauskaite, A., Ranson, A. & Sengpiel, F. Experience dependent plasticity of higher visual cortical areas in the mouse. *Cereb. Cortex* **33**, 9303–9312 (2023).
47. Zheng, X. et al. Host interneurons mediate plasticity reactivated by embryonic inhibitory cell transplantation in mouse visual cortex. *Nat. Commun.* **12**, 862 (2021).
48. Carceller, H., Guirado, R. & Nacher, J. Dark exposure affects plasticity-related molecules and interneurons throughout the visual system during adulthood. *J. Comp. Neurol.* **528**, 1349–1366 (2020).
49. Aronitz, E. M., Kamermans, B. A. & Duffy, K. R. Development of parvalbumin neurons and perineuronal nets in the visual cortex of normal and dark-exposed cats. *J. Comp. Neurol.* **529**, 2827–2841 (2021).
50. Reh, R. K. et al. Critical period regulation across multiple timescales. *Proc. Natl Acad. Sci. USA* **117**, 23242–23251 (2020).
51. Martinez, J. D. et al. Enriched binocular experience followed by sleep optimally restores binocular visual cortical responses in a mouse model of amblyopia. *Commun. Biol.* **6**, 408 (2023).
52. Kaneko, M. & Stryker, M. P. Sensory experience during locomotion promotes recovery of function in adult visual cortex. *eLife* **3**, e02798 (2014).
53. Kelly, K. R. et al. Improved binocular outcomes following binocular treatment for childhood amblyopia. *Investig. Ophthalmol. Vis. Sci.* **59**, 1221–1228 (2018).
54. Sengpiel, F. Plasticity of the visual cortex and treatment of amblyopia. *Curr. Biol. CB* **24**, R936–R940 (2014).
55. Castaldi, E., Lunghi, C. & Morrone, M. C. Neuroplasticity in adult human visual cortex. *Neurosci. Biobehav Rev.* **112**, 542–552 (2020).
56. Li, J. et al. The role of suppression in amblyopia. *Investig. Ophthalmol. Vis. Sci.* **52**, 4169–4176 (2011).

57. Maehara, G., Thompson, B., Mansouri, B., Farivar, R. & Hess, R. F. The perceptual consequences of interocular suppression in amblyopia. *Investig. Ophthalmol. Vis. Sci.* **52**, 9011–9017 (2011).
58. Levi, D. M. & Klein, S. A. Noise provides some new signals about the spatial vision of amblyopes. *J. Neurosci.* **23**, 2522–2526 (2003).
59. Huang, C., Tao, L., Zhou, Y. & Lu, Z.-L. Treated amblyopes remain deficient in spatial vision: A contrast sensitivity and external noise study. *Vis. Res.* **47**, 22–34 (2007).
60. Clavagnier, S., Dumoulin, S. O. & Hess, R. F. Is the cortical deficit in amblyopia due to reduced cortical magnification, loss of neural resolution, or neural disorganization? *J. Neurosci.* **35**, 14740–14755 (2015).
61. Joly, O. & Frankó, E. Neuroimaging of amblyopia and binocular vision: A review. *Front. Integr. Neurosci.* **8**, 62 (2014).
62. Wang, Y., Wu, Y., Luo, L. & Li, F. Structural and functional alterations in the brains of patients with anisometropic and strabismic amblyopia: A systematic review of magnetic resonance imaging studies. *Neural Regen. Res.* **18**, 2348–2356 (2023).
63. Levi, D. M. & Klein, S. A. Limitations on position coding imposed by undersampling and univariance. *Vis. Res.* **36**, 2111–2120 (1996).
64. Huh, C. Y. L. et al. Long-term monocular deprivation during juvenile critical period disrupts binocular integration in mouse visual thalamus. *J. Neurosci.* **40**, 585–604 (2020).
65. Shooner, C. et al. Asymmetric dichoptic masking in visual cortex of amblyopic macaque monkeys. *J. Neurosci.* **37**, 8734–8741 (2017).
66. Scholl, B., Pattadkal, J. J. & Priebe, N. J. Binocular disparity selectivity weakened after monocular deprivation in mouse v1. *J. Neurosci.* **37**, 6517–6526 (2017).
67. Hess, R. F., Wang, Y. Z., Demanins, R., Wilkinson, F. & Wilson, H. R. A deficit in strabismic amblyopia for global shape detection. *Vis. Res.* **39**, 901–914 (1999).
68. Hess, R. F. & Field, D. J. Is the spatial deficit in strabismic amblyopia due to loss of cells or an uncalibrated disarray of cells? *Vis. Res.* **34**, 3397–3406 (1994).
69. Baroncelli, L. et al. Enriched experience and recovery from amblyopia in adult rats: Impact of motor, social and sensory components. *Neuropharmacology* **62**, 2388–2397 (2012).
70. Sale, A. et al. Environmental enrichment in adulthood promotes amblyopia recovery through a reduction of intracortical inhibition. *Nat. Neurosci.* **10**, 679–681 (2007).
71. Ooi, T. L., Su, Y. R., Natale, D. M. & He, Z. J. A push-pull treatment for strengthening the 'lazy eye' in amblyopia. *Curr. Biol. CB* **23**, R309–R310 (2013).
72. Kiorpes, L. Understanding the development of amblyopia using macaque monkey models. *Proc. Natl Acad. Sci. USA* **116**, 26217–26223 (2019).
73. Stodieck, S. K., Greifzu, F., Goetze, B., Schmidt, K.-F. & Löwel, S. Brief dark exposure restored ocular dominance plasticity in aging mice and after a cortical stroke. *Exp. Gerontol*. **60**, https://doi.org/10.1016/j.exger.2014.09.007 (2014).
74. Sato, M. & Stryker, M. P. Distinctive features of adult ocular dominance plasticity. *J. Neurosci.* **28**, 10278–10286 (2008).
75. Ranson, A., Cheetham, C. E. J., Fox, K. & Sengpiel, F. Homeostatic plasticity mechanisms are required for juvenile, but not adult, ocular dominance plasticity. *Proc. Natl Acad. Sci. USA* **109**, 1311–1316 (2012).
76. Tagawa, Y., Kanold, P. O., Majdan, M. & Shatz, C. J. Multiple periods of functional ocular dominance plasticity in mouse visual cortex. *Nat. Neurosci.* **8**, 380–388 (2005).
77. Kalogeraki, E., Greifzu, F., Haack, F. & Löwel, S. Voluntary physical exercise promotes ocular dominance plasticity in adult mouse primary visual cortex. *J. Neurosci.* **34**, 15476–15481 (2014).
78. Meier, K. & Giaschi, D. Unilateral amblyopia affects two eyes: Fellow eye deficits in amblyopia. *Investig. Ophthalmol. Vis. Sci.* **58**, 1779–1800 (2017).
79. Agetsuma, M., Hamm, J. P., Tao, K., Fujisawa, S. & Yuste, R. Parvalbumin-positive interneurons regulate neuronal ensembles in visual cortex. *Cereb. Cortex* **28**, 1831–1845 (2018).
80. Saiepour, M. H. et al. Ocular dominance plasticity disrupts binocular inhibition-excitation matching in visual cortex. *Curr. Biol. CB* **25**, 713–721 (2015).
81. Donato, F., Rompani, S. B. & Caroni, P. Parvalbumin-expressing basket-cell network plasticity induced by experience regulates adult learning. *Nature* **504**, 272–276 (2013).
82. Vo, T. et al. The chemorepulsive axon guidance protein semaphorin3a is a constituent of perineuronal nets in the adult rodent brain. *Mol. Cell Neurosci.* **56**, 186–200 (2013).
83. Kepecs, A. & Fishell, G. Interneuron cell types are fit to function. *Nature* **505**, 318–326 (2014).
84. Knoblich, U., Huang, L., Zeng, H. & Li, L. Neuronal cell-subtype specificity of neural synchronization in mouse primary visual cortex. *Nat. Commun.* **10**, 2533 (2019).
85. Khan, A. G. et al. Distinct learning-induced changes in stimulus selectivity and interactions of gabaergic interneuron classes in visual cortex. *Nat. Neurosci.* **21**, 851–859 (2018).
86. Percie du Sert, N. et al. The arrive guidelines 2.0: Updated guidelines for reporting animal research. *PLoS Biol.* **18**, e3000410 (2020).
87. Goldey, G. J. et al. Removable cranial windows for long-term imaging in awake mice. *Nat. Protoc.* **9**, 2515–2538 (2014).
88. Prusky, G. T., Alam, N. M., Beekman, S. & Douglas, R. M. Rapid quantification of adult and developing mouse spatial vision using a virtual optomotor system. *Investig. Ophthalmol. Vis. Sci.* **45**, 4611–4616 (2004).
89. Abdeljalil, J. et al. The optomotor response: A robust first-line visual screening method for mice. *Vis. Res.* **45**, 1439–1446 (2005).
90. Kretschmer, F., Sajgo, S., Kretschmer, V. & Badea, T. C. A system to measure the optokinetic and optomotor response in mice. *J. Neurosci. Methods* **256**, 91–105 (2015).
91. La Chioma, A., Bonhoeffer, T. & Hübener, M. Disparity sensitivity and binocular integration in mouse visual cortex areas. *J. Neurosci.* **40**, 8883–8899 (2020).
92. Brainard, D. H. The psychophysics toolbox. *Spat. Vis.* **10**, 433–436 (1997).
93. Pachitariu, M. et al. Suite2p: beyond 10,000 neurons with standard two-photon microscopy. *bioRxiv* [Preprint]. https://doi.org/10.1101/061507 (2017).
94. Kerlin, A. M., Andermann, M. L., Berezovskii, V. K. & Reid, R. C. Broadly tuned response properties of diverse inhibitory neuron subtypes in mouse visual cortex. *Neuron* **67**, 858–871 (2010).

Acknowledgements

The authors thank Boxing Li, Jiali Li, Lingyi Zhang, Liling Liu, Xinyan Deng, Simin Zeng, and Juan Li for their contributions, which enabled some of the work reported here. This work was supported by the National Natural Science Foundation of China (Grant 82271115, 82471115 to M.Y.), Supporting Funds for SCI Paper Research (PT0009 to M.Y.), Guangdong Basic and Applied Basic Research Foundation (2023A1515011829 to Z.L.), Research Grants from the National Key R&D Program of China (Grants 2021YFF1200700 to L.H.).

Author contributions

Conceptualization: Y.R.H., Z.T.L., M.B.Y. Methodology: Y.R.H., Z.T.L., Z.Y.Z. Funding acquisition: Z.T.L., L.Y.H., M.B.Y. Project administration: Y.R.H., X.Y.Z., L.G., M.Q.W., Y.X.F. Supervision: Z.T.L., Z.Y.Z. Writing - original draft: Y.R.H. Writing - review & editing: L.Y.H., M.B.Y.

Competing interests

The authors declare no competing interests.

Additional information

Supplementary information The online version contains supplementary material available at https://doi.org/10.1038/s42003-024-07296-x.

Correspondence and requests for materials should be addressed to Lianyan Huang or Minbin Yu.

Peer review information *Communications Biology* thanks the anonymous reviewers for their contribution to the peer review of this work. Primary Handling Editor: Benjamin Bessieres. A peer review file is available.